

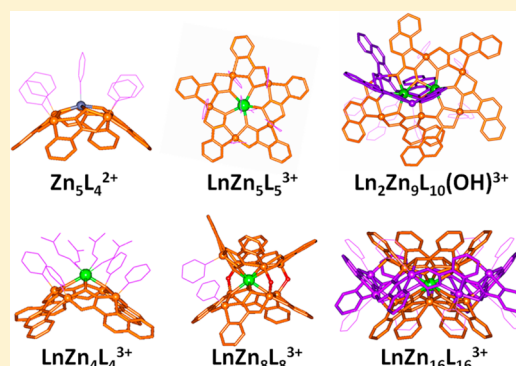
Solvent Dependent Assembly of Lanthanide Metallacrowns Using Building Blocks with Incompatible Symmetry Preferences

Joseph Jankolovits, Jeff. W. Kampf, and Vincent L. Pecoraro*

Chemistry Department, University of Michigan, 930 North University Avenue, Ann Arbor, Michigan 48109-1055, United States

Supporting Information

ABSTRACT: Solvent dependence in the assembly of coordination driven macrocycles is a poorly understood phenomenon. This work presents the solvent dependent assembly of 8 lanthanide metallacrowns (LnMCs) in solution using picoline hydroxamic acid (picHA), Zn(II), and Ln(III) ions. ESI-MS and single-crystal X-ray crystallography reveal the selective assembly of $\text{LnZn}_4(\text{picHA})_4^{3+}$, $\text{LnZn}_5(\text{picHA})_5^{3+}$, $\text{LnZn}_8(\text{picHA})_8^{3+}$, $\text{LnZn}_{12}(\text{picHA})_{12}^{3+}$, $\text{LnZn}_{16}(\text{picHA})_{16}^{3+}$, $\text{Ln}_2\text{Zn}_3(\text{picHA})_4^{4+}$, $\text{Ln}_2\text{Zn}_{7-9}(\text{picHA})_{8-10}$, and $\text{Ln}_4\text{Zn}_{4-5}(\text{picHA})_{8-9}$ complexes in five different solvents. The coordination preferences of the hard Ln(III) ion and relatively soft Zn(II) ion dictate the solvent selectivity in this system. The LnMCs assemble with open or closed Zn(II) and/or Ln(III) coordination sites based on the behavior of the solvent as an ancillary ligand. This structural promiscuity is attributed to the symmetry incompatible building blocks, which generate assemblies with substantial geometric strain such that no clear thermodynamic minimum exists between the different LnMCs. These LnMCs assemble from a $\text{Zn}_5(\text{picHA})_4^{2+}$ intermediate, which is monitored using ^1H NMR and ESI-MS to assess the stability of the complexes and possible assembly pathways based on kinetic considerations. LnMC assemblies that can be generated through central metal substitution reactions such as the $\text{LnZn}_4(\text{picHA})_4^{3+}$, $\text{LnZn}_5(\text{picHA})_5^{3+}$, and $\text{LnZn}_8(\text{picHA})_8^{3+}$ effectively reach equilibrium after 24 h at room temperature. In contrast, LnMCs that must disrupt the $\text{Zn}_5\text{L}_4^{2+}$ structure to assemble, such as the $\text{LnZn}_{16}\text{L}_{16}^{3+}$, reach equilibrium after heating for 24 h at 65 °C. A pathway for LnMC assembly is presented where the $\text{Zn}_5\text{L}_4^{2+}$ is the key intermediate based on these reaction data and shared structural motifs in the complexes. These results correlate solvent dependent assembly to the building block geometry, highlighting synthetic approaches for generating novel complexes.



INTRODUCTION

Dative bonds are used widely in the assembly of discrete supramolecular polygons, polyhedra, and helices.^{1–3} Interest in such coordination-driven complexes stems from their diverse architectures and physical properties. Interior cavities in many assemblies bind guests reversibly, allowing for fundamental studies of reactivity in confined spaces^{4,5} and perturbing the properties of responsive guests for sensing and molecular data storage.^{6–8} Coordination driven assemblies also serve as building blocks for the construction of porous solids, nanofibers, and liquid crystals.^{9–13} The metal ion building blocks can also impart catalytic, optical, magnetic, and electrochemical functionality.^{14–18}

Substantial research efforts have focused on controlling coordination-driven assembly, culminating in strategies for designing high symmetry macrocycles and polyhedra based on the geometry of the metal ion building blocks.^{19,20} One of the earliest classes of coordination driven macrocycles, metallacrowns (MCs) exemplify the use of symmetry considerations in the design of discrete macrocycles.^{21–24} MCs possess a repeating metal ion-heteroatom-heteroatom motif through the ring (Figure 1) and, analogous to crown ethers, frequently bind metal ions in their central cavity.^{25,26} MCs have drawn interest

as single-molecule magnets,^{27,28} near-infrared lumino-phores,^{29,30} molecular recognition agents,^{31–34} and building blocks for porous solids.^{35–38} Symmetry-based design strategies for MCs focus on the geometry of the fused-chelate rings in the ligand and the coordination preferences of the metal ions.³⁹ Ligands that form fused 5-membered and 6-membered chelate rings, such as salicylhydroxamic acid (shi^{3-}), orient metal ions at 90° angles. Furthermore, the equatorial arrangement of the chelate rings generates a linear edge. Thus, propagation of this chelate motif four times completes the 360° macrocycle and generates a square-shaped $[\text{12-MC}_{\text{M(N),L}}\text{-4}]$ (Figure 1).⁴⁰ Ligands that generate fused 5-membered chelate rings, such as picoline hydroxamic acid, generate a 72° angle between metal ions in the MC ring. With the appropriate ring metals and central metal, the building blocks complete the 360° rotation and generate a pentagonal $[\text{15-MC}_{\text{M(N),L}}\text{-5}]$. A planar arrangement of the bidentate ligands is important for generating the planar macrocycle. Jahn–Teller distorted ring metals, such as Cu(II), enforce a planar arrangement of chelate rings because ring strain on the elongated axis prevents the

Received: April 11, 2014

Published: June 23, 2014



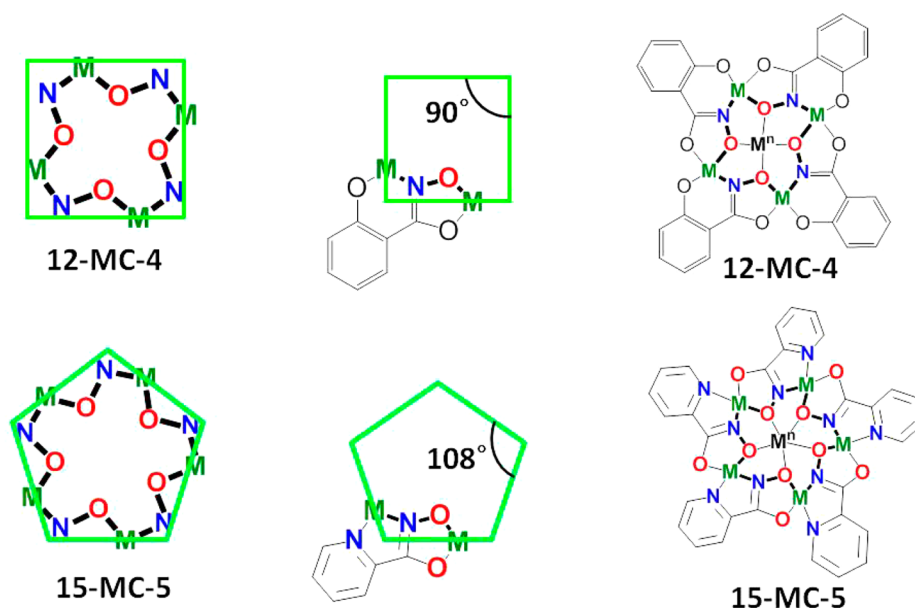


Figure 1. Diagrams displaying the design strategy for MCs based on the chelate ring geometry. The square-shaped $M(N)[12-MC_{M'(N'),L-4}]^{N+}$ is generated from ligands that form fused 5- and 6-membered chelate rings, such as salicylhydroximate (top). The pentagonal $M(N)[15-MC_{M'(N'),L-5}]^{N+}$ is generated from ligands that form fused 5-membered chelate rings, such as picHA (bottom).

formation of octahedral cis-isomers.^{41,42} Of note, Zn(II) has previously resulted in the formation of an unexpected inverse metallacrown.²⁴ The reliability of symmetry based MC design is evident in the reaction of picHA, an early Ln(III) ion, and either Cu(II) or Ni(II), which generates the $Ln(III)[15-MC_{M(II),picHA-5}]^{3+}$ complex exclusively.^{43–46}

In certain instances, a variety of assemblies can arise from identical components. Such structural promiscuity may result from flexible⁴⁷ or polytopic ligands,⁸ distortions in the metal ion geometry,^{48,49} solvation effects,^{50–54} guest recognition,^{17,55–59} or serendipity. This phenomenon can advantageously generate structurally responsive materials for sensing applications and novel complexes that cannot be predicted by symmetry-based design strategies. In general, however, our collective understanding of how a set of building blocks can yield multiple polynuclear assemblies is limited. Few guidelines for controlling the assembly of multiple coordination macrocycles have been established based on ligand design, metal coordination geometry, molecular recognition, or other external factors.

This work provides new insights into controlling the assembly of multiple coordination macrocycles from identical precursors through an investigation into the solvent dependent assembly of eight lanthanide metallacrowns (LnMCs) from the same three building blocks: picHA, Zn(II), and a Ln(III) ion. Five of these LnMCs have been crystallographically characterized. From these results, a design strategy is described for realizing and controlling structurally promiscuous assemblies. The approach utilizes symmetry incompatible building blocks with open coordination sites to direct the assembly of different structural motifs. Symmetry incompatible building blocks possess symmetry elements that are not complementary with a single self-assembled structure. Thus, each building block directs the assembly toward different constructs which possess notable geometric strain, so no motif has a strong thermodynamic preference. Furthermore, metal ions with open metal sites result in solvent coordination, or solvation, being the deciding factor in the assembly of a particular

construct. In this study, the geometry of the picHA ligand promotes the assembly of planar $Ln(III)[15-MC_{Zn(II),picHA-5}]^{3+}$ complexes. In contrast, the distorted square pyramidal geometry of Zn(II) leads to a nonplanar arrangement of equatorial picHA ligands, which promotes the formation of concave $Ln(III)[12-MC_{Zn(II),picHA-4}]^{3+}$ motifs. As Zn(II) and Ln(III) ions have open coordination sites, solvent interactions with the soft Zn(II) ring ions and hard Ln(III) ion dictate which macrocycle assembles. Insights into the stability and assembly pathways of these LnMCs are also discussed on the basis of ESI-MS and ¹H NMR data. Two of the LnMCs discussed in this work^{29,55} and two intermediates in their assembly⁵⁶ have been reported previously.

EXPERIMENTAL SECTION

All reagents were obtained from commercially available sources and used as received unless otherwise described. The ligands picHA²⁹ and quinHA⁵⁶ and the MC complexes $Zn_5(picHA)_4$,⁵⁶ $LnZn_5(picHA)_5$,⁵⁵ and $LnZn_{16}(picHA)_{16}$ ²⁹ were synthesized as previously described. Electrospray ionization mass spectrometry (ESI-MS) was performed with a Micromass LCT time-of-flight electrospray ionization mass spectrometer at 150 °C at cone voltages of 50 V. Samples were injected via syringe pump as ~50 μM solutions. ESI-MS data was processed with MassLynx 4.0 software. NMR spectroscopy was performed on 400 or 500 MHz Varian spectrometers and the chemical shifts referenced to residual solvent signals or the internal standards tetramethylsilane (TMS) or dioxane. ¹H Diffusion NMR spectroscopy was performed using the DOSY gradient compensated stimulated echo with spin lock and convection compensation (DgcsteSL_cc) pulse sequence at temperatures of 293 K in pyridine-D₅ and 293 or 298 K in methanol-D₄. A diffusion delay of 150 ms, diffusion gradient length of 3.0 ms, and a gradient strength array of 15–30 increments were used. The gradient field strength was calibrated with D₂O by the University of Michigan NMR facility staff. The data was fit according to the equation $\ln(I/I_0) = -\gamma^2 \delta^2 G^2 (\Delta - \delta/3) D$ to solve for the diffusion coefficient (D), where I = integral of the peak at a given G , I_0 = integral of the peak at $G = 0$, γ = magnetogyric constant of a hydrogen atom ($2.675 \times 10^8 \text{ T}^{-1} \text{ s}^{-1}$), δ = diffusion gradient length, Δ = diffusion delay, G = gradient field strength.

Table 1. Crystallographic Data for $\text{DyZn}_4(\text{quinHA})_4(\text{DMF})_4(\text{NO}_3)_3$, $\text{DyZn}_8(\text{picHA})_8(\text{OH})_3$, and $\text{Dy}_2\text{Zn}_9(\text{quinHA})_{10}(\text{OH})(\text{NO}_3)_{2.25}\text{Cl}_{0.75}$

complex	$\text{DyZn}_4(\text{quinHA})_4(\text{DMF})_4(\text{NO}_3)_3$	$\text{DyZn}_8(\text{picHA})_8(\text{OH})_3$	$\text{Dy}_2\text{Zn}_9(\text{quinHA})_{10}(\text{OH})(\text{NO}_3)_{2.25}\text{Cl}_{0.75}$
molecular formula	$\text{Dy}_{0.5}\text{Zn}_2\text{C}_{37.5}\text{H}_{45}\text{N}_9\text{O}_{13.5}$	$\text{DyZn}_8\text{C}_{60.5}\text{H}_{71.25}\text{N}_{18}\text{O}_{30.25}$	$\text{Dy}_2\text{Zn}_9\text{C}_{175.5}\text{H}_{167}\text{Cl}_{0.75}\text{N}_{31.25}\text{O}_{30.5}$
mol. wt [g mol^{-1}]	1056.82	2220.204	4141.82
cryst syst/space group	orthorhombic, $P2_12_12_1$	monoclinic, $P2_1/C$	triclinic, $\bar{P}1$
a [Å]	19.5887(5)	24.7224(5)	20.445(5)
b [Å]	22.7717(7)	22.7796(4)	21.830(5)
c [Å]	10.1759(3)	29.467(2)	22.271(5)
α [deg]	90	90	93.512(5)
β [deg]	90	110.143(8)	102.150(5)
γ [deg]	90	90	113.693(5)
vol [Å ³]	4539.1(1)	15579.6(12)	8779(4)
$Z/\text{density}, \rho$ [g cm^{-3}]	4/1.546	8/1.893	2/1.567
μ [mm^{-1}]/ $F(000)$	6.220/2150	8.514/8866	6.544/4195
cryst size [mm^3]	0.13 × 0.10 × 0.08	0.11 × 0.01 × 0.01	0.25 × 0.03 × 0.03
θ range for data collection [deg]	2.98–68.23	1.90–68.24	20.6–68.30
limiting indices	$-23 \leq h \leq 23$ $-27 \leq k \leq 27$ $-12 \leq l \leq 12$	$-29 \leq h \leq 29$ $-25 \leq k \leq 27$ $-35 \leq l \leq 35$	$-24 \leq h \leq 24$ $-26 \leq k \leq 26$ $-26 \leq l \leq 24$
measured/unique reflns	97529/8302	170675/28505	235204/31589
completeness to θ [%]	99.9	99.8	98.1
data/restraints/params	8302/166/628	28505/333/2206	31589/1952/2596
GOF on F^2	1.102	1.049	1.187
final R indices [$I > 2\sigma(I)$]	R1 = 0.0662, wR2 = 0.1831	R1 = 0.0832, wR2 = 0.2210	R1 = 0.0718, wR2 = 0.2058
R indices (all data)	R1 = 0.0704, wR2 = 0.1865	R1 = 0.1319, wR2 = 0.2605	R1 = 0.0794, wR2 = 0.2148
largest diff. peak and hole [$e \text{ \AA}^{-3}$]	1.165 and -1.076	2.667 and -2.304	1.514 and -3.124

$\text{LnZn}_4(\text{quinHA})_4^{3+}$. A general synthesis for these compounds is described below for the Dy(III) analogue. Complexes with other lanthanides were prepared by substituting the appropriate lanthanide ion for Dy(III). Characterization of all isolated complexes is provided after the synthetic exemplar.

$\text{DyZn}_4(\text{quinHA})_4(\text{NO}_3)_3$ – $\text{Dy(III)}[12\text{-MC}_{\text{Zn(II),quinHA-4}}](\text{NO}_3)_3$. QuinHA (0.133 mmol, 25.0 mg), zinc nitrate hexahydrate (0.133 mmol, 39.5 mg), and dysprosium nitrate hexahydrate (0.33 mmol, 14.6 mg) were combined in 3 mL of a 4:1 mixture of methanol and pyridine (v/v). Triethylamine (0.266 mmol, 37.1 μL) was added followed by the addition of 3 mL of dimethylformamide (DMF). Once homogeneous, the solution was immediately transferred to a 50 mL beaker and crystallized by ether vapor diffusion in a wide-mouth jar containing ~75 mL of ether. The yellow-orange crystals were isolated by filtration, rinsed with -20°C pyridine, and air-dried. Yield = 49.4 mg, 72%. ESI-MS (pyridine) gave $m/z = 614.9^{2+}$ (614.9²⁺ calcd for $[\text{DyZn}_4(\text{quinHA})_4(\text{NO}_3)_2]^{2+}$), 1290.8⁺ (1291.7⁺ calcd for $[\text{DyZn}_4(\text{quinHA})_4(\text{NO}_3)_2]^{+}$). CHN Analysis for $[(\text{DyZn}_4(\text{C}_{10}\text{H}_6\text{N}_2\text{O}_2)_4(\text{NO}_3)_3(\text{C}_5\text{H}_5\text{N})_4(\text{DMF})_4(\text{H}_2\text{O})_5)]$, found (calcd): C = 41.81 (42.11), H = 3.63 (4.03), N = 12.98 (12.96).

$\text{YZn}_4(\text{quinHA})_4(\text{NO}_3)_3$ – $\text{Y(III)}[12\text{-MC}_{\text{Zn(II),quinHA-4}}](\text{NO}_3)_3$. Yield = 43.1 mg, 65%. ESI-MS (pyridine) gave $m/z = 577.4^{2+}$ (578.4²⁺ calcd for $[\text{YZn}_4(\text{quinHA})_4(\text{NO}_3)_2]^{2+}$), 1216.7⁺ (1217.8⁺ calcd for $[\text{YZn}_4(\text{quinHA})_4(\text{NO}_3)_2]^{+}$). ¹H NMR δ (ppm) (500 MHz, 9:1 DMF-*D*₇/pyridine-*D*₅), 8.90 (d, 1H, $J = 9$ Hz), 8.56 (d, $J = 9$ Hz, 1H), 8.49 (d, 1H, $J = 9$ Hz), 8.20 (d, 1H, $J = 8$ Hz), 7.90 (t, 1H, $J = 8$ Hz), 7.73 (t, 1H, $J = 8$ Hz). CHN Analysis for $[(\text{YZn}_4(\text{C}_{10}\text{H}_6\text{N}_2\text{O}_2)_4(\text{NO}_3)_3(\text{C}_5\text{H}_5\text{N})_4(\text{DMF})_4(\text{H}_2\text{O})_{6.5})]$, found (calcd): C = 42.90 (43.09), H = 3.59 (4.27), N = 13.24 (13.26).

$\text{TbZn}_4(\text{quinHA})_4(\text{NO}_3)_3$ – $\text{Tb(III)}[12\text{-MC}_{\text{Zn(II),quinHA-4}}](\text{NO}_3)_3$. Yield = 39.7 mg, 27%. ESI-MS (9:1 DMF/pyridine (v/v)) gave $m/z = 613.5^{2+}$ (613.4²⁺ calcd for $[\text{TbZn}_4(\text{quinHA})_4(\text{NO}_3)_2]^{2+}$). CHN Analysis for $[(\text{TbZn}_4(\text{C}_{10}\text{H}_6\text{N}_2\text{O}_2)_4(\text{NO}_3)_3(\text{C}_5\text{H}_5\text{N})_4(\text{DMF})_4(\text{H}_2\text{O})_7)]$, found (calcd): C = 41.22 (41.46), H = 3.39 (4.16), N = 12.80 (12.76).

$\text{ErZn}_4(\text{quinHA})_4(\text{NO}_3)_3$ – $\text{Er(III)}[12\text{-MC}_{\text{Zn(II),quinHA-4}}](\text{NO}_3)_3$. Yield = 79.6 mg, 57%. ESI-MS (9:1 DMF/pyridine (v/v)) gave $m/z = 617.0^{2+}$ (617.9²⁺ calcd for $[\text{ErZn}_4(\text{quinHA})_4(\text{NO}_3)_2]^{2+}$). CHN Analysis

for $[(\text{ErZn}_4(\text{C}_{10}\text{H}_6\text{N}_2\text{O}_2)_4(\text{NO}_3)_3(\text{C}_5\text{H}_5\text{N})_4(\text{DMF})_4(\text{H}_2\text{O})_{6.5})]$, found (calcd): C = 41.31 (41.47), H = 3.49 (4.11), N = 12.65 (12.76).

$\text{LnZn}_8(\text{picHA})_8^{3+}$. $\text{LaZn}_8(\text{picHA})_8\text{Cl}_3$ – $\text{La(III)}[12\text{-MC}_{\text{Zn(II),picHA-4}}]_2\text{Cl}_3$. PicHA (100 mg, 0.724 mmol), zinc chloride (128.3 mg, 0.941 mmol), and $\text{La}(\text{NO}_3)_3$ hexahydrate (62.7 mg, 0.145 mmol) were mixed in 15 mL of a 9:1 water/pyridine mixture (v/v). After it was stirred overnight, the solution was set to slowly evaporate, yielding yellow crystals within 2 weeks. The crystals were isolated by filtration and rinsed with a -20°C solution of 4:1 water/pyridine. Yield = 60.0 mg, 16% based on picHA. ESI-MS (4:1 water/pyridine): 583.5³⁺ (583.5³⁺ calcd for $[\text{LaZn}_8(\text{C}_6\text{H}_4\text{N}_2\text{O}_2)_8]^{3+}$), 882.8²⁺ (883.8²⁺ calcd for $[\text{LaZn}_8(\text{C}_6\text{H}_4\text{N}_2\text{O}_2)_8(\text{OH})]^{2+}$), 893.8²⁺ (892.8²⁺ calcd for $\text{LaZn}_8(\text{C}_6\text{H}_4\text{N}_2\text{O}_2)_8\text{Cl}]^{2+}$). ¹H NMR δ (ppm) (400 MHz, 4:1 D_2O /pyridine-*D*₅), 8.45 (d, 1H, $J = 5$ Hz), 7.93 (m, 3H). CHN: found (calcd for $\text{LaZn}_8(\text{C}_6\text{H}_4\text{N}_2\text{O}_2)_8(\text{C}_5\text{H}_5\text{N})_{6.5}\text{Cl}_3(\text{H}_2\text{O})_{8.5}$) C = 38.55 (38.30), H = 3.10 (3.25), N = 11.91 (11.48).

$\text{DyZn}_8(\text{picHA})_8(\text{OH})_3$ – $\text{Dy(III)}[12\text{-MC}_{\text{Zn(II),picHA-4}}]_2(\text{OH})_3$. PicHA (100 mg, 0.724 mmol), zinc carbonate basic (79.5 mg, 0.724 mmol), and dysprosium carbonate (69.6 mg, 2.41 mmol) were mixed in 10 mL of a 9:1 water/pyridine mixture (v/v). After it was stirred overnight, the solution was filtered through a fine glass frit. The filtrate was set to crystallize by THF vapor diffusion. After 2 days, the solution was filtered to remove white precipitate and again set to crystallize by THF vapor diffusion. Yellow crystals formed within 2 weeks and were isolated by filtration and rinsed with a -20°C solution of 4:1 water/pyridine. Yield = 28.6 mg, 14% based on picHA. ESI-MS (4:1 water/pyridine): 895.2²⁺ (895.3²⁺ calcd for $\text{DyZn}_8(\text{C}_6\text{H}_4\text{N}_2\text{O}_2)_8(\text{OH})]^{2+}$). CHN: found (calcd for $\text{DyZn}_8(\text{C}_6\text{H}_4\text{N}_2\text{O}_2)_8(\text{C}_5\text{H}_5\text{N})_2(\text{OH})_3(\text{H}_2\text{O})_{15}$) C = 31.08 (30.91), H = 2.83 (3.35), N = 10.59 (11.19).

$\text{NdZn}_8(\text{picHA})_8(\text{OH})_3$ – $\text{Nd(III)}[12\text{-MC}_{\text{Zn(II),picHA-4}}]_2(\text{OH})_3$. The $\text{NdZn}_8(\text{picHA})_8(\text{OH})_3$ was synthesized following the procedure for $\text{DyZn}_8(\text{picHA})_8(\text{OH})_3$, substituting neodymium carbonate for dysprosium carbonate. Yield = 18.3 mg, 10% based on picHA. ESI-MS (4:1 water/pyridine): 585.9³⁺ (585.2³⁺ calcd for $\text{NdZn}_8(\text{C}_6\text{H}_4\text{N}_2\text{O}_2)_8]^{3+}$), 886.3²⁺ (886.3²⁺ calcd for $\text{NdZn}_8(\text{C}_6\text{H}_4\text{N}_2\text{O}_2)_8(\text{OH})]^{2+}$). CHN: found (calcd for $\text{NdZn}_8(\text{C}_6\text{H}_4\text{N}_2\text{O}_2)_8(\text{C}_5\text{H}_5\text{N})_2(\text{OH})_3(\text{H}_2\text{O})_{6.5}$) C = 33.66 (33.45), H = 2.65 (2.81), N = 11.55 (12.11).

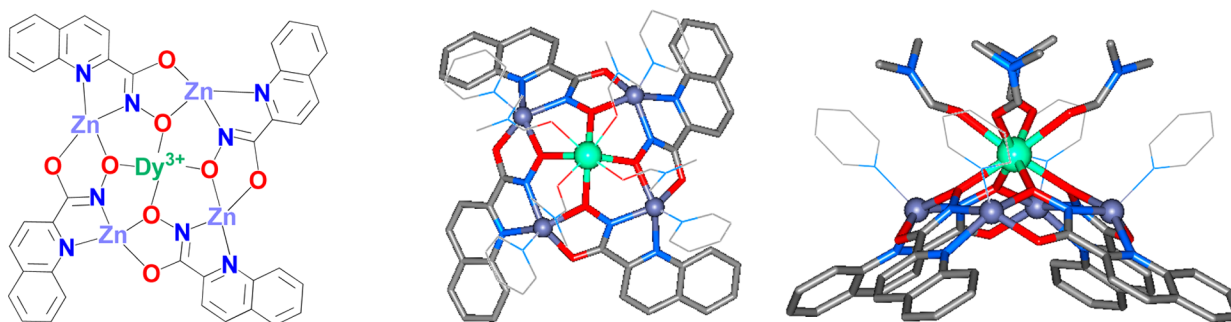


Figure 2. Chemdraw diagram (left) and crystal structure images of the $\text{DyZn}_4(\text{quinHA})_4(\text{DMF})_4(\text{NO}_3)_3(\text{py})_4$ complex. Color scheme: Gray = carbon, red = oxygen, blue = nitrogen, gray-purple = zinc, green = dysprosium. Coordinated pyridine and DMF (center only) ligands are displayed as thin lines for clarity.

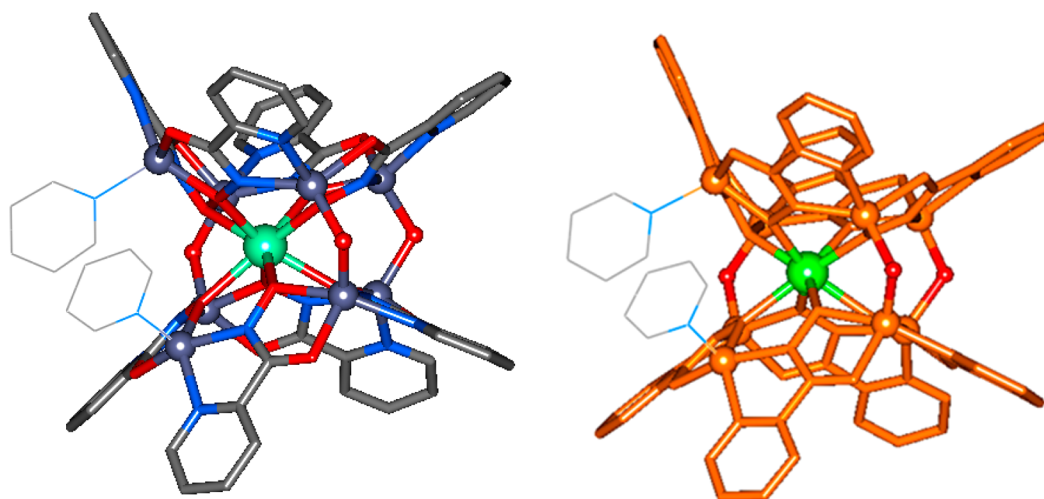


Figure 3. Crystal structure images of the $\text{DyZn}_8(\text{quinHA})_8(\text{OH})_3(\text{py})_2$ complex shown with elemental colors and in orange to highlight the $[\text{12-MC}_{\text{Zn(II),picHA-4}}]$ units. Color scheme: Gray = carbon, red = oxygen, blue = nitrogen, gray-purple = zinc, sea green, green = dysprosium, orange = atoms in the 12-MC-4. Coordinated pyridine ligands are displayed as thin lines for clarity.

$\text{Ln}_2\text{Zn}_9(\text{quinHA})_{10}(\text{OH})^{3+}$. A general synthesis for these compounds is described below for the Dy(III) analogue. Complexes with other lanthanides were prepared by substituting the appropriate lanthanide ion for Dy(III). Characterization of all isolated complexes is provided after the synthetic exemplar.

$\text{Dy}_2\text{Zn}_9(\text{quinHA})_{10}(\text{OH})(\text{NO}_3)_{2.25}\text{Cl}_{0.75}$. QuinHA (0.664 mmol, 125.0 mg), zinc chloride (0.531 mmol, 72.5 mg), triethylamine (1.33 mmol, 185 μL), and dysprosium nitrate hexahydrate (0.133 mmol, 58.2 mg) were stirred in 20 mL of a 1:1 mixture of water and pyridine (v/v). Once homogeneous, the solution was immediately transferred to a 50 mL beaker and crystallized by benzene vapor diffusion in a wide-mouth jar containing ~ 75 mL of benzene. Yellow-orange crystals were isolated by filtration, rinsed with a 4 $^\circ\text{C}$ 4:1 mixture of water and pyridine (v/v), and air-dried. Yield = 166.1 mg, 67% based on H_2quinHA . ESI-MS (4:1 water/pyridine (v/v)) gave $m/z = 930.5^{3+}$ (930.3^{3+} calcd for $[\text{Dy}_2\text{Zn}_9(\text{quinHA})_{10}(\text{OH})]^{3+}$), CHN Analysis for $[\text{Dy}_2\text{Zn}_9(\text{C}_{10}\text{H}_6\text{N}_2\text{O}_2)_{10}(\text{OH})\text{Cl}_{0.5}(\text{NO}_3)_{2.5}(\text{C}_5\text{H}_5\text{N})_8(\text{H}_2\text{O})_9]$, found (calcd) C = 44.60 (44.80), H = 3.00 (3.20), N = 11.28 (11.28).

$\text{Tb}_2\text{Zn}_9(\text{quinHA})_{10}(\text{OH})(\text{NO}_3)_{2.25}\text{Cl}_{0.75}$. Yield = 158.5 mg, 63% based on H_2quinHA . ESI-MS (4:1 water/pyridine (v/v)) gave $m/z = 928.4^{3+}$ (928.2^{3+} calcd for $[\text{Tb}_2\text{Zn}_9(\text{quinHA})_{10}(\text{OH})]^{3+}$), CHN Analysis for $[\text{Tb}_2\text{Zn}_9(\text{C}_{10}\text{H}_6\text{N}_2\text{O}_2)_{10}(\text{OH})\text{Cl}_{0.5}(\text{NO}_3)_{2.5}(\text{C}_5\text{H}_5\text{N})_7(\text{H}_2\text{O})_9]$, found (calcd) C = 44.02 (44.22), H = 2.84 (3.13), N = 11.26 (11.17).

$\text{Eu}_2\text{Zn}_9(\text{quinHA})_{10}(\text{OH})(\text{NO}_3)_{2.25}\text{Cl}_{0.75}$. Yield = 168.5 mg, 68% based on H_2quinHA . ESI-MS (4:1 water/pyridine (v/v)) gave $m/z = 923.4^{3+}$ (923.5^{3+} calcd for $[\text{Eu}_2\text{Zn}_9(\text{quinHA})_{10}(\text{OH})]^{3+}$), CHN Analysis for $[\text{Eu}_2\text{Zn}_9(\text{C}_{10}\text{H}_6\text{N}_2\text{O}_2)_{10}(\text{OH})\text{Cl}_{0.75}(\text{NO}_3)_{2.25}(\text{C}_5\text{H}_5\text{N})_{7.5}(\text{H}_2\text{O})_8]$, found (calcd) C = 44.80 (44.94), H = 2.85 (3.14), N = 11.43 (11.34).

X-ray Crystallography. Intensity data for the structures were collected at 85(2) K on an AFC10K Saturn 944+ CCD-based X-ray diffractometer equipped with a low temperature device and Micromax-007HF Cu-target microfocus rotating anode ($\lambda = 1.54187$ Å), operated at 0.20 kW power (20 kV, 10 mA), $\mu = 4.510$ mm^{-1} . The data were processed with CrystalClear 2.0⁵⁷ and corrected for absorption. The structures were solved and refined with the SHELXTL (version 2008/4) software package.⁵⁸ All non-hydrogen atoms were refined anisotropically with the hydrogen atoms placed at their ideal positions. All other experimental details are presented in Table 1.

RESULTS

LnMC Crystal Structures. Previous work reported the crystallization of $\text{Ln(III)}[\text{15-MC}_{\text{Zn(II),picHA-5}}](\text{NO}_3)_3$ ($\text{LnZn}_5(\text{picHA})_5(\text{NO}_3)_3$) and $\text{Ln(III)}[\text{12-MC}_{\text{Zn(II),picHA-4}}]_2[\text{24-MC}_{\text{Zn(II),picHA-8}}](\text{OTf})_3$ ($\text{LnZn}_{16}(\text{picHA})_{16}(\text{OTf})_3$) complexes.⁵⁵ Three novel LnMC motifs were crystallized in this work with Zn(II) and Ln(III) ions. Picoline hydroxamic acid was the primary ligand in this study. However, a less-soluble structural derivative, quinaldic hydroxamic acid (quinHA), was also utilized to facilitate LnMC crystallization when appropriate crystallization conditions could not be identified with picHA. Notably, the $\text{Zn}_5\text{L}_4^{2+}$ has been crystallographically characterized with both ligands and no substantial structural differences could be elucidated between the two complexes.⁵⁶ Therefore, the structures of the LnMCs

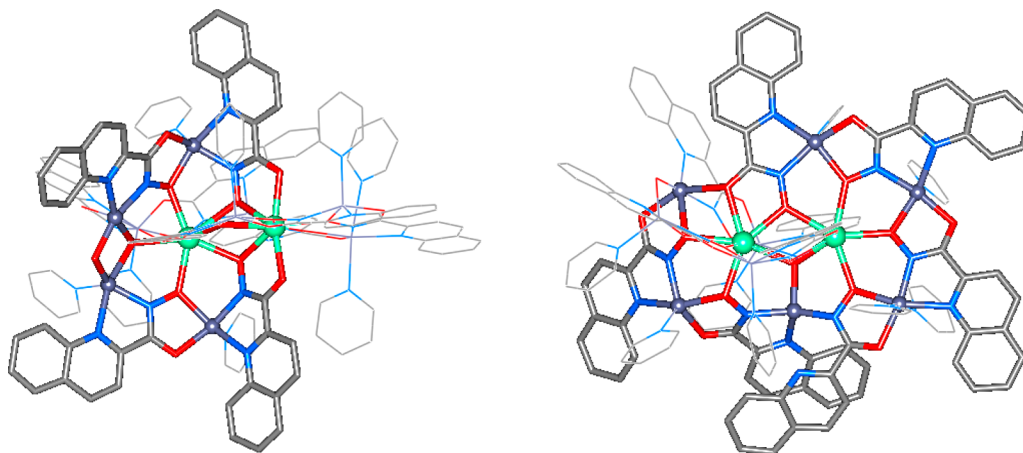


Figure 4. Crystal structure images of the $\text{Dy}_2\text{Zn}_9(\text{quinHA})_{10}(\text{OH})(\text{py})_9(\text{NO}_3)_{2.25}\text{Cl}_{0.75}$ complex displayed from two different angles to highlight the $[\text{14-MC}_{\text{Zn(II),quinHA-5}}]$ (left) and split $[\text{15-MC}_{\text{Zn(II),quinHA-5}}]$ (right) motifs. Color scheme: Gray = carbon, red = oxygen, blue = nitrogen, gray-purple = zinc, sea green = dysprosium. Coordinated pyridine ligands are displayed as thin lines for clarity.

with quinHA should be representative of the motifs assembled with picHA in solution.

First, a $\text{Dy(III)}[\text{12-MC}_{\text{Zn(II),quinHA-4}}](\text{DMF})_4(\text{NO}_3)_3$ complex ($[\text{DyZn}_4(\text{quinHA})_4(\text{NO}_3)_3]$, Figure 2) was crystallized by ether vapor diffusion into a DMF/pyridine solution. The complex shows the distinct $[\text{Zn-N-O}]$ repeat unit of a MC repeated 4-fold in a macrocycle, with a Dy(III) ion in the center bound to the $\text{O}_{\text{hydroximate}}$. The ditopic ligand bridges the Zn(II) ring ions with bidentate $\text{N}_{\text{hydroximate}}/\text{N}_{\text{pyridyl}}$ and $\text{O}_{\text{hydroximate}}/\text{O}_{\text{carbonyl}}$ chelates. As a whole, the complex is a Ln(III) analogue of the previously reported $\text{Zn(II)}[\text{12-MC}_{\text{Zn(II),quinHA-4}}](\text{BF}_4)_2$.⁵⁶ Each Zn(II) ion is five coordinate with pyridine ligands bound axially. To assign whether the ions are square pyramidal or trigonal bipyramidal, τ -values were measured, where 0 = pure square pyramidal and 1 = pure trigonal bipyramidal.⁶⁹ τ -values of 0.08–0.22 indicate the Zn(II) ring ions have square pyramidal geometry. The Zn(II) ions rest above the ligand plane by 0.564 Å on average. Elongated Zn(II)– $\text{N}_{\text{quinHA-pyridyl}}$ bond distances of 2.21 Å are observed. The central cavity on the $\text{Dy(III)}[\text{12-MC}_{\text{Zn(II),quinHA-4}}](\text{DMF})_4(\text{NO}_3)_3$ has a radius of merely 0.64 Å, too small for the 1.027 Å radius of Dy(III). Therefore, the Dy(III) ion sits 1.19 Å above the oxygen mean plane. The Dy(III) is 8-coordinate, possessing four DMF ligands. The Dy– $\text{O}_{\text{hydroximate}}$ bond distances are slightly shorter than the Dy– O_{DMF} distances (2.330 and 2.406 Å, respectively). Three unbound nitrate anions in the lattice provide charge balance. This complex was also isolated with Y(III), Tb(III), and Er(III) lanthanide ions.

A crystal structure of a $\text{Dy(III)}[\text{12-MC}_{\text{Zn(II),picHA-4}}]_2(\text{OH})_3(\text{py})_2$ sandwich complex was obtained from aqueous pyridine solutions and carbonate salts of Zn(II) and Dy(III). In the structure, three μ_2 -oxygen atoms bridge the axial positions of the Zn(II) ring metals (Figure 3). These bridging oxygens are assigned as hydroxides based on the acidity of the two Zn(II) ions, requirements for charge neutrality, and the somewhat short Zn–O bond lengths (av = 1.981 Å). The average Zn–O–Zn angle of 108° is more consistent with the sp^3 hybridization expected for water, however this can be attributed to strain imposed by the staggered $[\text{12-MC}_{\text{Zn(II),picHA-4}}]$ units. The two Zn(II) ions without hydroxide ligands are adjacent to each other and have axially bound pyridines. The pitch of the picHA ligands varies around the ring, which is reflected in the range of τ -values found in the Zn(II) ions

(0.01–0.76). This pitch variation is attributed to the different axial ligands on the Zn(II) ring ions. The complex as a whole is the dimeric sandwich complex of the $\text{LnZn}_4(\text{quinHA})_4^{3+}$ described above. In addition, such a sandwich motif was observed in the previously reported $\text{LnZn}_{16}(\text{picHA})_{16}^{3+}$ encapsulated sandwich complex. A $\text{NdZn}_8(\text{picHA})_8(\text{OH})_3$ complex was also isolated. An analogous $\text{LaZn}_8(\text{picHA})_8\text{Cl}_3$ structure was obtained without bridging hydroxide ligands. However, substantial disorder prevented the complete refinement of this structure.

Lastly, a crystal structure of a dilanthanide complex was obtained with the quinHA ligand, $\text{Dy}_2\text{Zn}_9(\text{quinHA})_{10}(\text{OH})(\text{py})_9(\text{NO}_3)_{2.25}\text{Cl}_{0.75}$ (Figure 4). The $\text{Dy}_2\text{Zn}_9(\text{quinHA})_{10}(\text{OH})^{3+}$ possesses two 8-coordinate Dy(III) ions in the center that are bridged by three μ_2 - $\text{O}_{\text{hydroximate}}$ atoms. The MC repeat unit propagates irregularly around this core. The complex appears as two planar LnMCs that have collided at a 90° angle relative to the other. On one, a distinct $\text{Dy(III)}[\text{14-MC}_{\text{Dy(III),Zn(II),quinHA-5}}](\text{OH})$ motif possessing only C_2 rotational symmetry is observed. The $\text{Dy(III)}[\text{14-MC}_{\text{Dy(III),Zn(II),quinHA-5}}]$ motif contains a Dy(III) ring metal at one end and a μ_2 -oxygen bridge at the other. Such a $\text{Dy(III)}[\text{14-MC}_{\text{Dy(III),Mn(III),shi-5}}](\text{OH})^{2+}$ motif was recently reported with Mn(III) ring metals and shi ligands (Figure 5).²⁸ The bridging oxygen is thought to be a hydroxide based on the charge balance requirements for the +4 charged cluster, as only three negative charges can be assigned in the lattice. ESI-MS of the complex also consistently shows a hydroxide adduct (vide infra). The 1.99 and 1.95 Å Zn–O bond distances and 101.5° Zn–O–Zn bond angles do not clarify whether the oxygen is a water or hydroxide. Hydrogen bond acceptors surrounding the oxygen atom demonstrate that the oxygen is protonated, however the assignment as a hydroxide or water based on the orientation of the hydrogen bond acceptors is not possible due to disorder. From this evidence, the oxygen atom is tentatively assigned as a hydroxide, though formulation as a water ligand is possible. The other portion of the $\text{Dy}_2\text{Zn}_9(\text{quinHA})_{10}$ structure could be described as a partially formed $\text{Dy(III)}[\text{15-MC}_{\text{Zn(II),quinHA-5}}]$ (Figure 5 and Supporting Information S1). Four Zn(II) ions and four quinHA ligands propagate the prototypical MC motif. However, a Dy(III) ion occupies the position of the fifth zinc, disrupting the macrocycle. The fourth Zn(II) ion is four-coordinate, binding

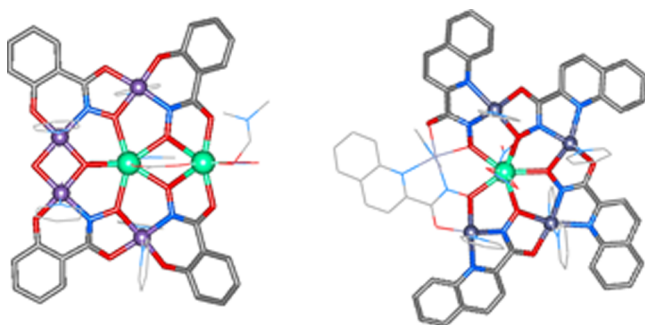


Figure 5. Depictions of the Ln(III)[14-MC_{Mn(III),shi-5}](OH)²⁺²⁸ (left) and Dy(III)[15-MC_{Zn(II),quinHA-5}] (right, Supporting Information) complexes for comparison with the structural motifs in the Dy₂Zn₉(quinHA)₁₀(OH)(py)₉(NO₃)_{2,25}Cl_{0,75}. Color scheme: Gray = carbon, red = oxygen, blue = nitrogen, gray-purple = zinc, sea green = dysprosium, purple = manganese.

the fifth quinHA ligand with an opposite directionality as the other ligands. The O,O'-chelate of this quinHA ligand binds to an additional Zn(II)-quinHA subunit, which altogether caps the axial metal sites on the Dy(III)[14-MC_{Dy(III),Zn(II),quinHA-5}]. The Ln₂Zn₉(quinHA)₁₀(OH)³⁺ was also isolated with Tb(III) and Eu(III) ions.

Solvent Dependent LnMC Assembly. ESI-MS characterization of LnMC assembly reactions was performed in different solvents in order to demonstrate the solvent selectivity of the assembly process. For this study, H₂picHA, triethylamine, Zn(NO₃)₂, and Ln(NO₃)₃ (Ln = La(III), Y(III)) were mixed in a 5:10:5:1 ratio with the concentration of Ln(NO₃)₃ being 5.8 mM. These standard reaction conditions were employed in all solvents to demonstrate that the selective assembly is not a result of the stoichiometry, concentration, or counterion differences. Reactions were performed at room temperature and 65 °C for 24 h to identify complexes that have higher activation energies for assembly. Both La(III) and Y(III) were examined to assess templating effects based on the size of the Ln(III) ion (8-coordinate ionic radii = 1.16 and 1.02 Å, respectively). It was expected that this size discrepancy could greatly impact the thermodynamic stability of the LnMC because La(III) has a 1.57 greater log K for displacing Ca(II) from a Ca(II)[15-MC_{Cu(II),pheHA-5}]³⁺ than Y(III).⁵⁹ Also, the diamagnetism of La(III) and Y(III) benefits the NMR experiments below. The assembly reactions performed in pyridine, 9:1 DMF/pyridine, 4:1 water/pyridine, methanol, and DMF at room temperature and 65 °C are described. Performing the reaction in DMSO, acetonitrile, and pure water did not result in appreciable LnMC formation and, therefore, are not discussed. For each solvent, the species identified in the assembly reactions are listed in Table 2. It should be noted that ESI-MS peak intensities are dependent on the ionization efficiency of the ion, which varies depending on the chemical species and the solution conditions. The peak intensities listed herein are meant to describe the appearance of the spectra and not to draw conclusions about the relative concentrations of the MC complexes.

ESI-MS analysis of the reaction between picHA, Zn(II), and La(III) in pyridine at room temperature reveals the LaZn₅(picHA)₅³⁺ as the predominant LnMC product. Peaks for LaZn₅(picHA)₅(NO₃)₂²⁺ at *m/z* = 603.3²⁺ and LaZn₅(picHA)₅(NO₃)₂⁺ at *m/z* = 1268.5 are present with 100% and 56% relative intensity (Supporting Information Figure S2). Various other LaZn₅(picHA)₅³⁺ adducts with hydroxide anions

Table 2. MC Species Observed by ESI-MS for the Reaction of H₂picHA, Triethylamine, Zn(NO₃)₂, and Ln(NO₃)₃ (5:10:5:1 Ratio) in the Indicated Solvent^a

solvent	MCs w/o Ln(III)	La(III) MCs	Y(III) MCs
pyridine	Zn ₅ L ₄	LaZn ₄ L ₄	YZn ₄ L ₄
		LaZn₅L₅	YZn₅L₅
		LaZn ₄ L ₅	YZn ₄ L ₄
9:1 DMF/pyridine	Zn ₅ L ₄	LaZn ₄ L ₄	YZn ₄ L ₄
		LaZn₅L₅	YZn₅L₅
4:1 water/pyridine	Zn ₅ L ₄	LaZn ₅ L ₅	YZn ₈ L ₈
		LaZn₈L₈	Y₂Zn₇L₈
		La ₂ Zn ₉ L ₁₀	Y₂Zn₈L₉
			Y₂Zn₈L₁₀
methanol	Zn ₅ L ₄ Zn ₁₃ L ₁₁ Zn ₁₄ L ₁₂	LaZn₅L₅	YZn₁₆L₁₆
		LaZn₁₆L₁₆	Y ₄ Zn ₄ L ₈
			Y ₄ Zn ₅ L ₉
DMF	Zn ₅ L ₄ Zn ₁₄ L ₁₂ Zn ₁₅ L ₁₃	LaZn ₄ L ₄	YZn ₄ L ₄
		LaZn₅L₅	YZn ₈ L ₈
		LaZn ₈ L ₈	YZn₁₂L₁₂
		LaZn₁₂L₁₂	YZn ₁₆ L ₁₆
		LaZn₁₆L₁₆	Y ₂ Zn ₃ L ₄

^aThe LnMC species with the greatest relative intensities are displayed in bold.

or coordinated solvent molecules are also present in the mass spectrum. Furthermore, peaks for Zn₅(picHA)₄²⁺ and a LaZn₄(picHA)₄³⁺ species can also be seen with about 1% relative intensity (Table 2). ESI-MS analysis of the standard assembly reaction in 9:1 DMF/pyridine led to an increase in the relative intensity of the LaZn₄(picHA)₄³⁺ to 8% after heating the reaction at 65 °C for 24 h, though LaZn₅(picHA)₅(NO₃)₂²⁺ is still the greatest intensity peak (Figure 6 and Supporting Information Figure S2).

ESI-MS of 5:10:5:1 mixtures of picHA, triethylamine, Zn(NO₃)₂, and La(NO₃)₃ salts in 4:1 water/pyridine (v/v) at room temperature (Figure 6 and Supporting Information Figure S2) reveals peaks for LaZn₈(picHA)₈³⁺ at 582.8 *m/z* and 38% relative intensity and LaZn₈(picHA)₈(OH)²⁺ at 883.8 *m/z* and 100% relative intensity. In addition, a Zn₅(picHA)₄²⁺ peak has 49% intensity and an La₂Zn₉(picHA)₁₀(OH)³⁺ species was identified at 747.5 *m/z* with 11% relative intensity. Upon heating the reaction mixture for 24 h at 65 °C, no new species grow into the spectrum, though the relative intensity of the Zn₅(picHA)₄²⁺ peak increases to 100% and the LnMC peaks concomitantly decrease in intensity. In methanol, peaks for the LaZn₅(picHA)₅(NO₃)₂²⁺ at *m/z* = 603.3²⁺ have the greatest intensity after reacting at room temperature and 65 °C for 24 h, though a strong LaZn₁₆(picHA)₁₆³⁺ species persists as well at *m/z* = 1120.7. In DMF, the room temperature assembly reaction shows the LaZn₅(picHA)₅³⁺ as the predominant species, though LaZn₈(picHA)₈(NO₃)₂²⁺ peak at 906.3 *m/z* has 21% relative intensity (Supporting Information Figure S2). Performing the reaction in DMF at 65 °C results in a dramatically different spectrum (Figure 6). While the LaZn₅(picHA)₅³⁺ as a significant species, the LaZn₈(picHA)₈³⁺ species is no longer present. Instead, peaks corresponding to LaZn₁₂(picHA)₁₂(NO₃)(OH)(H⁺)₂²⁺ at 878.9 and LaZn₁₆(picHA)₁₆³⁺ at 1120.7 *m/z* are evident with 61% and 32% relative intensity, respectively.

Performing the assembly reaction with Y(NO₃)₃ in place of La(NO₃)₃ results in largely the same species and solvent trends (Supporting Information Figure S4 and Figure 6). However,

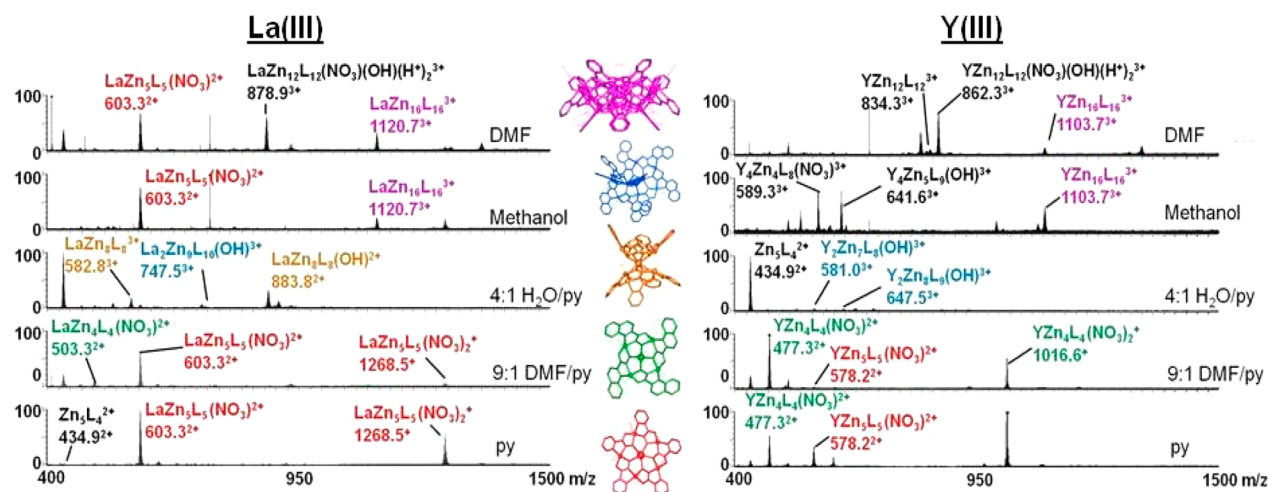


Figure 6. Mass spectra of assembly reactions performed at 65 °C of 5:10:5:1 H₂picHA, triethylamine, Zn(NO₃)₂, and either La(NO₃)₃ (left) or Y(NO₃)₃ (right) in the indicated solvents after 24 h. The peak labels are color coded with the structures of the corresponding crystallographically characterized complexes. In the peak labels, L = picHA.

the relative intensities of the species vary, presumably due to different thermodynamic stabilities of the LnMCs based on the size of the Ln(III) ion (vide infra). ESI-MS of the assembly reaction between picHA, triethylamine, Zn(NO₃)₂, and Y(NO₃)₃ (5:10:5:1 ratio) with Y(III) in pyridine reveals the Zn₅(picHA)₄²⁺ species at *m/z* = 434.9²⁺ is the predominant species with 100% relative intensity. Peaks for YZn₄(picHA)₄³⁺ and YZn₅(picHA)₅³⁺ species are observed at room temperature with less than 5% relative intensity (Supporting Information Figure S4). After heating at 65 °C for 24 h, these peaks increase in intensity such that the YZn₄(picHA)₄³⁺, YZn₄(picHA)₄(NO₃)₂²⁺, and YZn₅(picHA)₅³⁺ species have 56%, 100%, and 43% relative intensity, respectively, while the Zn₅(picHA)₄²⁺ peak intensity drops to 10%. In 9:1 DMF/pyridine, the YZn₄(picHA)₄³⁺ peak intensity relative to the YZn₅(picHA)₅³⁺ species is greater compared to pyridine. After heating at 65 °C, the YZn₄(picHA)₄³⁺ at 477.3 *m/z* has 100% intensity while the YZn₅(picHA)₅³⁺ peak at 578.2 *m/z* has 4% intensity (Figure 6).

The assembly reaction at room temperature in 4:1 H₂O/pyridine (v/v) with Y(III) reveals strong peaks for dilanthanide complexes, such as a Y₂Zn₈(picHA)₁₀(OH)³⁺ at *m/z* 647.5 and 40% relative intensity and Y₂Zn₉(picHA)₁₀²⁺ at *m/z* = 1029.8 and 59% relative intensity. Additionally, a YZn₈(picHA)₈(OH)²⁺ 859.0 *m/z* is evident with 9% intensity. Performing the reaction at 65 °C results in similar peaks but much lower intensity (<10%) relative to the Zn₅(picHA)₄²⁺ species at 434.9²⁺. In methanol, the room temperature reaction reveals peaks for a Y₂Zn₃(picHA)₄(NO₃)₃²⁺ species at 520.9 with 72% intensity, Zn₁₄(picHA)₁₂(methoxide)³⁺ at 860.7 *m/z* with 30% intensity, and YZn₁₆(picHA)₁₆³⁺ at 1103.7 *m/z* with 34% intensity. Performing the reaction at 65 °C results in the loss of the Y₂Zn₃(picHA)₄(NO₃)₃²⁺ peaks and the appearance of Y₄Zn₄(picHA)₈(NO₃)₃³⁺ at 589.3 *m/z* with 78% relative intensity and Y₄Zn₅(picHA)₉(OH)³⁺ at 641.6 *m/z* with 76% relative intensity. In DMF, the ESI-MS spectrum of the assembly reaction at room temperature reveals a mixture of Zn₅(picHA)₄²⁺, YZn₄(picHA)₄³⁺, YZn₈(picHA)₈³⁺, and Y₂Zn₃(picHA)₄⁴⁺ species. However, ESI-MS analysis of the assembly reaction in DMF at 65 °C for 24 h reveals the loss of these species and the growth of peaks for YZn₁₂(picHA)₁₂³⁺ at 834.3 *m/z* with 8% intensity, YZn₁₂(picHA)₁₂(NO₃)(OH)-

(H⁺)₂³⁺ at 862.3 *m/z* with 74% intensity, and YZn₁₆(picHA)₁₆³⁺ at 1103.7 *m/z* with 13% intensity.

On the basis of this intricate solvent dependence in the assembly of LnMCs, the solvent dependence of Zn₅(picHA)₄²⁺ was examined. Previously, the Zn₅(picHA)₄²⁺ was the only MC found to assemble in pyridine based on ESI-MS. The reaction between picHA, triethylamine, and Zn(NO₃)₂ in a 1:2:1 mixture was performed in a variety of solvents (Supporting Information Figure S5). In all pyridine containing solvents, the Zn₅(picHA)₄²⁺ at 434.9 *m/z* was the only MC that could be identified in the mass spectra. In methanol, the mass spectrum revealed peaks at *m/z* = 860.7³⁺ and 1307.5²⁺, corresponding to Zn₁₄(picHA)₁₂(methoxide)³⁺ and Zn₁₄(picHA)₁₂(methoxide)-(NO₃)²⁺ species, respectively. Peaks for Zn₁₃(picHA)₁₁⁴⁺ and Zn₁₅(picHA)₁₃⁴⁺ species were also observed with less than 20% relative intensity. Similar peaks were seen when the assembly was performed in DMF, though with less than 5% intensity relative to the Zn₅L₄²⁺ peaks. Unfortunately, these complexes have not been crystallographically characterized yet. Observation of such a large cluster is not unprecedented as a Cu₂₈(α-aminoHA)₂₀(OAc)₁₀Cl₄²⁺ helicate has been isolated from methanol.⁷⁰

Conversion of Zn₅(picHA)₄²⁺ to LnMCs. The reaction of the Zn₅(picHA)₄²⁺ with Ln(III) ions was assessed to provide qualitative insights into the kinetics of the assembly of the different LnMCs, the thermodynamic stability relative to the Zn₅(picHA)₄²⁺, and support the role of the Zn₅(picHA)₄²⁺ as an intermediate in the assembly of the LnMCs.⁵⁶ The reactions were performed by adding 0.8 equiv of either La(NO₃)₃ or Y(NO₃)₃ to the Zn₅(picHA)₄(OTf)₂, which gives a 5:6.25:1 ratio of picHA, Zn(II), and the Ln(III). ¹H NMR and ESI-MS were collected after 24 h at room temperature and 24 h of heating at 65 °C. The titration of La(III) and Y(III) to the Zn₅(picHA)₄(OTf)₂ in pyridine were previously reported.⁵⁵ These titrations show over 90% conversion of the Zn₅(picHA)₄²⁺ to the LaZn₅(picHA)₅³⁺ at room temperature after 24 h, and 99% conversion after heating at 65 °C for 24 h. The reaction with Y(III) is not as complete or selective. The Zn₅(picHA)₄²⁺ remains as a major species in solution after heating at 65 °C for 24 h, and more than one new LnMC product is present.

In 9:1 DMF/pyridine, conversion of the $\text{Zn}_5(\text{picHA})_4^{2+}$ to L_nMCs occurs readily at room temperature. With La(III), ESI-MS shows the $\text{LaZn}_5(\text{picHA})_5^{3+}$ is the primary product of the reaction (Supporting Information Figure S5). Four downfield resonances grow into the ^1H NMR spectrum at room temperature, though the $\text{Zn}_5(\text{picHA})_4^{2+}$ is still present with a 3.5:1 integral ratio of $\text{LaZn}_5(\text{picHA})_5^{3+}$ to $\text{Zn}_5(\text{picHA})_4^{2+}$. No changes are observed upon heating the spectrum at 65 °C for 24 h. In 4:1 water/pyridine, very little conversion of the $\text{Zn}_5(\text{picHA})_4^{2+}$ to the $\text{LaZn}_8(\text{picHA})_8^{3+}$ occurs with the addition of 0.8 equiv of $\text{La}(\text{NO}_3)_3$ (Supporting Information Figure S6) at room temperature or 65 °C. The ^1H NMR spectra shows very low intensity peaks that grow in at ~8.5 and 8.1 ppm that are consistent with the spectrum of isolated $\text{LaZn}_8(\text{picHA})_8^{3+}$, though with the integral ratio relative to the $\text{Zn}_5(\text{picHA})_4^{2+}$ being 0.05:1 or less. ESI-MS reveals low intensity peaks for the $\text{LaZn}_8(\text{picHA})_8^{3+}$, supporting that limited conversion occurs.

In methanol, ^1H NMR and ESI-MS demonstrate that the $\text{Zn}_5(\text{picHA})_4^{2+}$ reacts with La(III) to form both the $\text{LaZn}_5(\text{picHA})_5^{3+}$ and the $\text{LaZn}_{16}(\text{picHA})_{16}^{3+}$ (Supporting Information Figure S7). Upon reacting at room temperature for 24 h, the $\text{LaZn}_5(\text{picHA})_5^{3+}$ to $\text{LaZn}_{16}(\text{picHA})_{16}^{3+}$ to $\text{Zn}_5(\text{picHA})_4^{2+}$ ^1H NMR integral ratio are 0.8:0.01:1. The mass spectra shows a modest, 2% relative intensity for the $\text{LaZn}_{16}(\text{picHA})_{16}^{3+}$ at 1120.7 m/z . Heating the reaction mixture at 65 °C for 24 h leads to the growth of the $\text{LaZn}_{16}(\text{picHA})_{16}^{3+}$ peaks in the ^1H NMR and ESI-MS spectra. The resonance integral ratios for $\text{LaZn}_5(\text{picHA})_5^{3+}$ to $\text{LaZn}_{16}(\text{picHA})_{16}^{3+}$ to $\text{Zn}_5(\text{picHA})_4^{2+}$ reaches 0.5:0.5:1. In DMF, the addition of 0.8 equiv of $\text{La}(\text{NO}_3)_3$ to the $\text{Zn}_5(\text{picHA})_4^{2+}$ results in downfield resonances for the $\text{LaZn}_5(\text{picHA})_5^{3+}$ appearing after 24 h with a 1.2:1 integral ratio relative to the $\text{Zn}_5(\text{picHA})_4^{2+}$ (Supporting Information Figure S8). ESI-MS supports that the $\text{Zn}_5(\text{picHA})_4^{2+}$ and $\text{LaZn}_5(\text{picHA})_5^{3+}$ are the only major species in solution. Upon heating the solution at 65 °C for 24 h, the $\text{LaZn}_5(\text{picHA})_5^{3+}$ to $\text{Zn}_5(\text{picHA})_4^{2+}$ integral ratio shifts to 1:1. In addition, a variety of low intensity peaks grow in to the ^1H NMR spectrum between 6.8 and 9.2 ppm. ESI-MS shows a prominent peak for the $\text{LaZn}_{12}(\text{picHA})_{12}(\text{NO}_3)(\text{OH})(\text{H}^+)_2^{3+}$ at 878.8 m/z and 45% intensity and a peak for the $\text{LaZn}_{16}(\text{picHA})_{16}^{3+}$ at 1120.7 m/z with less than 5% intensity. In summary, $\text{Zn}_5\text{L}_4^{2+}$ conversion to the $\text{LaZn}_5(\text{picHA})_5^{3+}$ or $\text{LaZn}_8(\text{picHA})_8^{3+}$ proceeds readily at room temperature, while the $\text{LaZn}_{12}(\text{picHA})_{12}^{3+}$ and $\text{LaZn}_{16}(\text{picHA})_{16}^{3+}$ formation requires heating.

The reaction between the $\text{Zn}_5(\text{picHA})_4^{2+}$ and $\text{Y}(\text{NO}_3)_3$ in 9:1 DMF/pyridine yields the $\text{YZn}_4(\text{picHA})_4^{3+}$ is the primary product based on ESI-MS (Supporting Information Figure S9), where a $\text{YZn}_4(\text{picHA})_4(\text{NO}_3)_2^{2+}$ peak at $m/z = 477.3$ has 100% intensity relative to the $\text{Zn}_5(\text{picHA})_4^{2+}$ at 434.9 m/z with 20% intensity. In the ^1H NMR spectrum, the $\text{YZn}_4(\text{picHA})_4^{3+}$ resonances are slightly upfield of the $\text{Zn}_5(\text{picHA})_4^{2+}$ signals, with a 3.9:1 integral ratio. These integral ratios are effectively unchanged upon heating at 65 °C for 24 h. These data show that there is no significant energy barrier inhibiting $\text{Zn}_5(\text{picHA})_4^{2+}$ conversion to the $\text{LaZn}_5(\text{picHA})_5^{3+}$ and $\text{YZn}_4(\text{picHA})_4^{3+}$. In 4:1 H_2O /pyridine, the titration of $\text{Y}(\text{III})$ to the $\text{Zn}_5(\text{picHA})_4^{2+}$ results in the near complete loss of the $\text{Zn}_5(\text{picHA})_4^{2+}$ resonances and the appearance of a variety of peaks with very low intensity (Supporting Information Figure S10). The ESI-MS spectrum of this reaction mixture contains a $\text{Zn}_5(\text{picHA})_4^{2+}$ peak at 434.9 m/z and 100% relative intensity.

Peaks for the $\text{YZn}_8(\text{picHA})_8^{3+}$ and Y_2 clusters are also evident with less than 10% relative intensity. The low intensity of the resonances in the ^1H NMR spectrum could be due to the low concentration of the different species in solution or exchange processes. No significant changes to the ^1H NMR or ESI-MS spectra are evident after heating the reaction mixture for 24 h at 65 °C.

Reacting the $\text{Zn}_5(\text{picHA})_4(\text{OTf})_2$ with $\text{Y}(\text{NO}_3)_3$ in methanol at room temperature results in very weak peaks for the $\text{YZn}_{16}(\text{picHA})_{16}^{3+}$ appearing in the mass spectrum at 1103.7 m/z with less than 5% intensity and the ^1H NMR spectrum with roughly a 0.05:1 integral ratio with the $\text{Zn}_5(\text{picHA})_4^{2+}$ (Figure 7). After heating the reaction mixture at 65 °C for 24 h, the

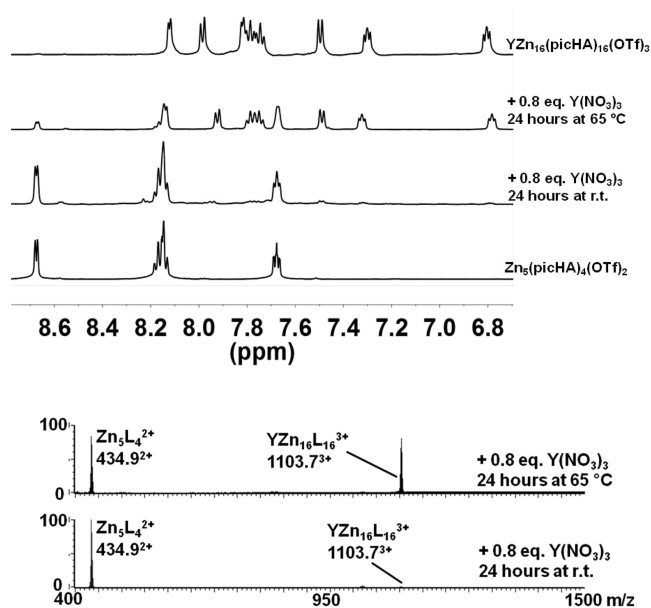


Figure 7. ^1H NMR and ESI-MS spectra of the titration of 0.8 equiv of $\text{Y}(\text{NO}_3)_3$ to $\text{Zn}_5(\text{picHA})_4(\text{OTf})_2$ in methanol- D_4 .

$\text{YZn}_{16}(\text{picHA})_{16}^{3+}$ peaks dramatically increase in intensity. The $\text{YZn}_{16}(\text{picHA})_{16}^{3+}$ to $\text{Zn}_5(\text{picHA})_4^{2+}$ integral ratios in the ^1H NMR spectrum are 2.75:1, and the ESI-MS peaks for the two species have roughly equal intensity. Furthermore, the ESI-MS and ^1H NMR spectra show no evidence for the $\text{YZn}_5(\text{picHA})_5^{3+}$. Thus, the reaction of the $\text{Zn}_5(\text{picHA})_4^{2+}$ with $\text{Y}(\text{III})$ in methanol proceeds selectively to the $\text{YZn}_{16}(\text{picHA})_{16}^{3+}$, though the $\text{LaZn}_5(\text{picHA})_5^{3+}$ also forms with $\text{La}(\text{III})$. In DMF, the addition $\text{Y}(\text{NO}_3)_3$ to the $\text{Zn}_5(\text{picHA})_4^{2+}$ leads to significant changes to the ^1H NMR spectrum (Supporting Information Figure S11) after 24 h at room temperature. A resonance at 8.65 ppm appears with a 2.25:1 integral ratio relative to the $\text{Zn}_5(\text{picHA})_4^{2+}$. ESI-MS suggests this species is the $\text{YZn}_4(\text{picHA})_4^{3+}$, though peaks for the $\text{YZn}_8(\text{picHA})_8^{3+}$ and $\text{YZn}_{16}(\text{picHA})_{16}^{3+}$ are also observed with less than 10% intensity. Upon heating, the ^1H NMR spectrum shows nearly complete loss of the $\text{Zn}_5(\text{picHA})_4^{2+}$. The $\text{YZn}_4(\text{picHA})_4^{3+}$ also loses intensity, and new resonances appear from 6.8–9.2 ppm. ESI-MS reveals that these new resonances originate from the $\text{YZn}_{12}(\text{picHA})_{12}^{3+}$ and $\text{YZn}_{16}(\text{picHA})_{16}^{3+}$. So the conversion of the $\text{Zn}_5(\text{picHA})_4^{2+}$ to the $\text{YZn}_4(\text{picHA})_4^{3+}$ proceeds at room temperature, though appreciable formation of larger MCs requires heating.

Solution Stability and Interconversion of the Lanthanide MCs. As many practical applications of coordination

driven assemblies occur in solution, the solution stability of the various LnMCs was assessed. While all LnMCs discussed in this work assemble with both La(III) and Y(III) based on ESI-MS, not all complexes could be isolated with all of the lanthanide ions. Furthermore, many complexes could only be crystallized with the quinHA ligand, presumably because of the lower solubility of the larger aromatic group in these polar solvents. Direct comparisons of solution stability and interconversion were complicated by these factors.

Previously, the $\text{LnZn}_5(\text{picHA})_5^{3+}$ complexes were shown to be stable in methanol and pyridine at room temperature over a period of 24 h. However, the complexes show evidence for rearranging in solution over 2 weeks, as peaks for the $\text{Zn}_5(\text{picHA})_4^{2+}$, $\text{LnZn}_{16}(\text{picHA})_{16}^{3+}$, and dinuclear Ln_2 clusters appear in ESI-MS spectra of these solutions. In 4:1 water/pyridine, the $\text{LnZn}_5(\text{picHA})_5^{3+}$ complexes rapidly convert to the $\text{LnZn}_8(\text{picHA})_8^{3+}$ and Ln_2 clusters within 2 h. The $\text{LnZn}_{16}(\text{picHA})_{16}^{3+}$ was found to be stable in methanol, pyridine, and DMF. However, rearrangement of the $\text{LnZn}_{16}(\text{picHA})_{16}^{3+}$ to the $\text{LnZn}_8(\text{picHA})_8^{3+}$ can be observed by ESI-MS within 24 h in 4:1 water/pyridine at room temperature.

The $\text{LnZn}_4(\text{quinHA})_4^{3+}$ partially converts to the $\text{LnZn}_5(\text{quinHA})_5^{3+}$ and $\text{Zn}_5(\text{quinHA})_4^{2+}$ in 9:1 DMF/pyridine based on ESI-MS. ^1H NMR spectra of the $\text{YZn}_4(\text{quinHA})_4^{3+}$ after 5 min in solution show the complex is the only major species (Supporting Information Figure S12). After 26 h at room temperature, a new species with 20% relative integrals grows in. ESI-MS suggests this new species is the $\text{Zn}_5(\text{quinHA})_4^{2+}$. The $\text{LaZn}_8(\text{picHA})_8^{3+}$ displays limited stability in solution as it partially degrades to the $\text{Zn}_5(\text{picHA})_4^{2+}$ after 24 h in 4:1 H_2O /pyridine, though no other LnMCs are present (Supporting Information Figure S13). The ^1H NMR spectrum of the $\text{LaZn}_8(\text{picHA})_8\text{Cl}_3$ shows two distinct MC resonances at 8.65 and 7.93 ppm with relative integrals of 1:3 (Supporting Information Figure S6). In methanol, the complex completely rearranges to form the $\text{LaZn}_5(\text{picHA})_5^{3+}$ and $\text{LaZn}_{16}(\text{picHA})_{16}^{3+}$ after 24 h at room temperature. Conversion to the $\text{LaZn}_5(\text{picHA})_5^{3+}$ is evident by ESI-MS in pyridine or to the $\text{LaZn}_{16}(\text{picHA})_{16}^{3+}$ in 9:1 DMF/pyridine and DMF at room temperature in 24 h. The $\text{Ln}_2\text{Zn}_9(\text{quinHA})_{10}(\text{OH})^{3+}$ shows limited solution stability as well. The mass spectrum contains peaks for the complex only in 4:1 water/pyridine upon dissolution for 15 min (Supporting Information Figure S13), though peaks for the $\text{Zn}_5(\text{quinHA})_4^{2+}$ appear within 24 h at room temperature. The complex rearranges to other dilanthanide species in methanol after 24 h at room temperature, though rearrangement is not seen in pyridine or 9:1 DMF/pyridine.

DISCUSSION

Solvent Directed Assembly of Symmetry Incompatible Building Blocks with Open Coordination Sites. This work establishes the intricate solvent-dependence that controls the assembly of LnMCs with picHA and Zn(II) ions. A key aim of this work is to extract principles for controlling solvent dependence based on the building block geometry. Such solvent dependence may advantageously lead to responsive assemblies for sensing applications or realize novel complexes that could not be designed by the prevailing symmetry-based design strategies for coordination driven assemblies. Of note, LnMCs can display single molecule magnetism, molecular recognition behavior, and second harmonic generation. LnMCs

with Zn(II) ring ions exhibit bright near-infrared luminescence because the MC topology excludes C–H oscillators from the proximity of the lanthanide ion, which mitigates vibrational quenching.^{29,30}

Crucial to understanding the solvent dependent assembly seen with Zn(II) ring ions, there is no solvent dependence in the assembly of the $\text{LnCu}_5(\text{picHA})_5^{3+}$ and $\text{LnNi}_5(\text{picHA})_5^{3+}$. The lack of solvent dependence in these complexes is attributed to the symmetry compatible building blocks. The equatorial coordination preferences of Cu(II) and Ni(II) and the geometry of picHA share an enthalpic preference for the planar pentagonal complex. Therefore, other LnMCs do not assemble because of the significant strain involved in forming the $\text{Ln(III)[12-MC}_{\text{M(II),picHA-4}}]^{3+}$ or other motifs with these building blocks. Importantly, $\text{LnCu}_5(\text{picHA})_5^{3+}$ and $\text{LnNi}_5(\text{picHA})_5^{3+}$ do not exhibit solvent dependence even though they have solvent-accessible coordination sites. This observation demonstrates that the open coordination sites alone do not lead to solvent dependent assembly behavior.

Alternatively, solvent dependence is observed using the symmetry incompatible building blocks picHA, Zn(II), and Ln(III). PicHA generates the vertex of a planar pentagon and Zn(II) forms nonplanar 5-coordinate complexes. The Ln(III) ions readily adopt C_3 , C_4 , and C_5 symmetrical coordination environments with almost no thermodynamic preference. Therefore, these building blocks do not share the symmetry elements of a single self-assembled complex. In other words, there is no single motif that can be assembled that avoids geometric strain. Since the Zn(II) and Ln(III) ions have open coordination sites, the assembly of these building blocks is influenced by their interactions with solvent molecules. It should be noted that the solvent is also acting as a ligand in these complexes, so the effects of solvation and coordination to the open metal sites cannot be separated.

Solvent Directed Assembly of PicHA, Zn(II), and Ln(III). ESI-MS provides the strongest evidence for the selectivity imposed by the solvent. By simply mixing H_2picHA , 2 equiv of triethylamine to facilitate ligand deprotonation, and 1 equiv of $\text{Zn}(\text{NO}_3)_2$, two distinct MC structural motifs assemble in solution (Supporting Information Figure S4): the $\text{Zn}_5(\text{picHA})_4^{2+}$ and clusters with approximately $\text{Zn}_{14}(\text{picHA})_{12}^{4+}$ formulations. Upon mixing 5 equiv of H_2picHA , 10 equiv of triethylamine, 5 equiv of $\text{Zn}(\text{NO}_3)_2$, and 1 equiv of a $\text{Ln}(\text{NO}_3)_3$ salt, eight distinct LnMC motifs have been identified that assemble in solution (Figure 6, Supporting Information Figures S2 and S3, and Table 2): $\text{LnZn}_4(\text{picHA})_4^{3+}$, $\text{LnZn}_5(\text{picHA})_5^{3+}$, $\text{LnZn}_8(\text{picHA})_8^{3+}$, $\text{LnZn}_{12}(\text{picHA})_{12}^{3+}$, $\text{LnZn}_{16}(\text{picHA})_{16}^{3+}$, $\text{Ln}_2\text{Zn}_3(\text{picHA})_4^{4+}$, $\text{Ln}_2\text{Zn}_{7-9}(\text{picHA})_{8-10}$, and $\text{Ln}_4\text{Zn}_{4-5}(\text{picHA})_{8-9}$. Excepting the $\text{Ln}_2\text{Zn}_3(\text{picHA})_4^{4+}$, all complexes persist after heating the solutions at 65 °C for 24 h and have been observed with both Y(III) and La(III). Six of these MCs have been isolated and crystallographically characterized with either picHA or quinHA ligands: $\text{Zn}_5(\text{picHA})_4^{2+}$, $\text{LnZn}_4(\text{quinHA})_4^{3+}$, $\text{LnZn}_5(\text{picHA})_5^{3+}$, $\text{LnZn}_8(\text{picHA})_8^{3+}$, $\text{LnZn}_{16}(\text{picHA})_{16}^{3+}$, and $\text{Ln}_2\text{Zn}_9(\text{quinHA})_{10}(\text{OH})^{3+}$.

The geometry of the fused chelate rings on picHA promotes the formation of a pentagonal $[\text{15-MC}_{\text{Zn(II),picHA-5}}]$ motif (Figure 1). Therefore, the $\text{LnZn}_5(\text{picHA})_5^{3+}$ assembly is directed by the ligand and it assembles in all solvents (Table 2). In contrast, the distorted square pyramidal Zn(II) ring metals promote the formation of concave $[\text{12-MC}_{\text{Zn(II),picHA-4}}]$ topologies. Additionally, it can be surmised that aqueous

pyridine mixtures lead to bridging waters or hydroxides, as seen in the $\text{DyZn}_8(\text{picHA})_8(\text{OH})_3$ and $\text{Dy}_2\text{Zn}_9(\text{quinHA})_{10}(\text{OH})^{3+}$ structures (Figures 3 and 4). On the basis of the assembly data, selectivity for the $\text{LnZn}_4(\text{picHA})_4^{3+}$, $\text{LnZn}_8(\text{picHA})_8^{3+}$, Ln_2 clusters, $\text{LnZn}_{12}(\text{picHA})_{12}^{3+}$, and $\text{LnZn}_{16}(\text{picHA})_{16}^{3+}$ is dictated by solvent interactions with the metal ions.

Figure 8 relates the solvent to the LnMCs that selectively assemble in those conditions. The $\text{LnZn}_5\text{L}_5^{3+}$ was omitted from

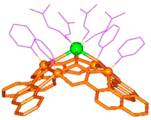
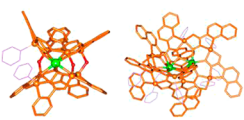
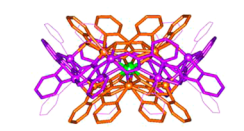
		Solvents that Coordinate to Ln(III) (DMF)	
		Present	Not Present
Solvents that Coordinate to Zn(II) (pyridine w/o water)	Present	LnZn_4L_4 	LnZn_8L_8 Ln_2 Clusters 
	Not Present	$\text{LnZn}_{12}\text{L}_{12}$ $\text{Ln}_2\text{Zn}_3\text{L}_4$	$\text{LnZn}_{16}\text{L}_{16}$ Ln_4 Clusters 

Figure 8. Relationship between the predominant LnMCs that selectively assemble after 24 h at 65 °C in solution based on the presence of DMF and/or pyridine. The $\text{LnZn}_5\text{L}_5^{3+}$ was omitted since it assembles to some extent in all solvents surveyed in this work.

this chart as its assembly shows a limited solvent dependence. It is evident that pyridine containing solvents lead to the formation of complexes with solvent exposed Zn(II) ions, such as the $\text{LnZn}_4\text{L}_4^{3+}$ and $\text{LnZn}_8\text{L}_8^{3+}$. This trend likely arises from the Zn(II) ring metal having a high affinity for pyridine, which both have intermediate softness. Hydroxide, and presumably water as well, can act as a bridging ligand between two Zn(II) ions. Therefore, the assembly in 4:1 water/pyridine

generates MCs with solvent-exposed Zn(II) ring metals and bridging hydroxides. This selectivity is reflected in the crystal structure of the $\text{DyZn}_8(\text{picHA})_8(\text{OH})_3$ complex (Figure 3), which contains Zn(II) ions with pyridine or hydroxides in the axial positions.

The Ln(III) ions are more oxophilic than Zn(II), preferring to interact with DMF. This preference for DMF is reflected in the preferential assembly of the $\text{LnZn}_4\text{L}_4^{3+}$ in 9:1 DMF/pyridine. The Ln(III) ions are exposed to the DMF molecules while the Zn(II) ring metals are free to interact with pyridine. The DMF ligands on the central Dy(III) ion in the $\text{DyZn}_4(\text{quinHA})_4(\text{DMF})_4(\text{NO}_3)_3$ crystal structure are consistent with this trend (Figure 2). In 4:1 water/pyridine, there is no DMF to solvate the exposed Ln(III) sites in the $\text{LnZn}_4\text{L}_4^{3+}$. Therefore, a sandwich motif is generated to saturate the coordination sphere of the central Ln(III) ion. The assembly of the $\text{LnZn}_{16}\text{L}_{16}$ in methanol, which contains a sandwich motif, further supports this idea that DMF prevents Ln(III)[12-MC $_{\text{Zn(II),L-4}}$] $_2$ sandwich motifs. Furthermore, the [24-MC $_{\text{Zn(II),L-8}}$] motif in the $\text{LnZn}_{16}\text{L}_{16}^{3+}$ can be attributed to the absence of pyridine during its assembly. As the Zn(II) ions are not solvated by pyridine, the 24-MC-8 assembles to bind to the Zn(II) axial coordination sites. In summary, DMF solvates the Ln(III) coordination sites and prevents the formation of sandwich complexes. Pyridine solvates the axial Zn(II) sites and blocks the formation of [24-MC $_{\text{Zn(II),L-8}}$] motifs on the Ln(III)[12-MC $_{\text{Zn(II),L-4}}$] $^{3+}$.

While a crystal structure of the $\text{LnZn}_{12}\text{L}_{12}^{3+}$ complex that preferentially assembles in DMF could not be obtained, these assembly trends suggest it has a Ln(III)[12-MC $_{\text{Zn(II),L-4}}$][24-MC $_{\text{Zn(II),L-8}}$](DMF) $_4^{3+}$ structure. A model of this proposed structure was prepared by manually removing one [12-MC $_{\text{Zn(II),picHA-4}}$] subunit from the $\text{DyZn}_{16}(\text{picHA})_{16}(\text{OTf})_3$ structure and then overlaying central Dy ion with the Dy(DMF) $_4$ subunit of the $\text{DyZn}_4(\text{quinHA})_4(\text{DMF})_4(\text{NO}_3)_3$ complex such that sensible bond distances and angles were maintained in the program Discovery Studio Visualizer 2.5.⁶⁰ This model is displayed in Figure 9 and Supporting Information Figure S14, showing the Ln(III)[12-

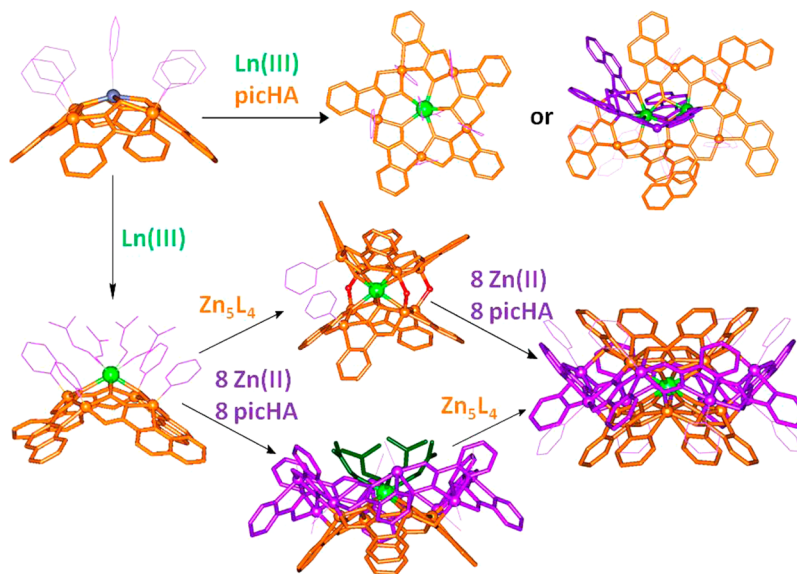


Figure 9. A minimal scheme depicting pathways for the conversion of the $\text{Zn}_5\text{L}_4^{2+}$ to LnMCs. The proposed structure for the $\text{LnZn}_{12}(\text{picHA})_{12}(\text{DMF})_4^{3+}$ species is displayed at the bottom with DMF ligands in dark green.

$\text{MC}_{\text{Zn(II),picHA-4}}^{3+}$ motif with four DMF ligands coordinated to the Ln(III) ion, just as in the $\text{DyZn}_4(\text{quinHA})_4(\text{DMF})_4(\text{NO}_3)_3$ structure. A $[24\text{-MC}_{\text{Zn(II),L-8}]$ is expected to bind the Zn(II) ions of the $[12\text{-MC}_{\text{Zn(II),L-4}]$ since there is no pyridine to solvate the axial coordination sites on the ring metals.

It is also worth considering the $\text{Zn}_{14}\text{L}_{12}^{4+}$ complex that assembles in methanol and DMF, but not in pyridine containing solvents. Considering that a $[24\text{-MC}_{\text{Zn(II),picHA-8}]$ assembles on the Ln(III) $[12\text{-MC}_{\text{Zn(II),picHA-4}]_2^{3+}$ motif of the $\text{LnZn}_{16}(\text{picHA})_{16}^{3+}$ in methanol, it is possible that this $\text{Zn}_{14}\text{L}_{12}^{4+}$ species contains a Zn(II) $[12\text{-MC}_{\text{Zn(II),L-4}][24\text{-MC}_{\text{Zn(II),L-8}]^{2+}$ structure. Such a complex would have a $\text{Zn}_{13}\text{L}_{12}^{2+}$ stoichiometry. While a species with this stoichiometry has not been observed by ESI-MS, it is possible that the species can only be ionized with an exogenous Zn(II) to form the $\text{Zn}_{14}\text{L}_{12}^{4+}$, or by losing a ligand to form the $\text{Zn}_{13}\text{L}_{11}^{4+}$.

The strategy of using symmetry incompatible building blocks with open coordination sites should be quite general because similar symmetry considerations dictate the assembly of most MCs and other coordination driven assemblies. Systems with only one metal ion would be expected to form only two coordination motifs, which is seen in the $\text{Zn}_5\text{L}_4^{2+}$ and $\text{Zn}_{14}\text{L}_{12}^{4+}$ assembled from Zn(II) and picHA. As picHA, Zn(II), and Ln(III) is a three component system, a greater number of complexes are observed. Moreover, *differential* solvation preferences of the soft Zn(II) ions and hard Ln(III) ions likely contributes to the assembly of so many complexes in this system. If both metal ions had similar polarizabilities, they would have similar interactions with the solvent and the assembly process might not be perturbed as significantly as this system.

Insights into the Assembly Mechanism. Analysis of the structures and $\text{Zn}_5\text{L}_4^{2+}$ reactivity data provides insights into the LnMC assembly pathways. We are proposing the following pathways depicted in Figure 9, where the $\text{Zn}_5\text{L}_4^{2+}$ is the key intermediate in LnMC assembly and undergoes three types of reactions: (1) Insertion of a Ln(III) ion into the center of the MC, pushing the central Zn(II) into the ring of a split-open $[12\text{-MC}_{\text{Zn(II),L-4}]$, (2) substitution of the central Zn(II) ion in the $\text{Zn}_5\text{L}_4^{2+}$ for a Ln(III) ion, and (3) cannibalization of the $\text{Zn}_5\text{L}_4^{2+}$ to abstract Zn(II) and picHA ligands that reassemble on an LnMC template. We feel that two distinct pathways will lead to different types of LnMCs using these three reactions.

Performing the first reaction on the $\text{Zn}_5\text{L}_4^{2+}$, where the Ln(III) ion disrupts the $[12\text{-MC}_{\text{Zn(II),L-4}]$ by pushing the central Zn(II) into the ring, could generate the $\text{LnZn}_5\text{L}_5^{3+}$ upon the incorporation of an exogenous ligand to complete the split-open macrocycle. This concept is supported by the observation of the split-open Ln(III) $[15\text{-MC}_{\text{Zn(II),quinHA-5}]$ motif in the $\text{Dy}_2\text{Zn}_9(\text{quinHA})_{10}(\text{OH})^{3+}$ structure (Figure 4). Additionally, dilanthanide clusters such as the $\text{Ln}_2\text{Zn}_9\text{L}_{10}(\text{OH})^{3+}$ may be generated from this split-open LnMC species.

The second pathway invokes the central ion substitution reaction to replace the central Zn(II) ion of the $\text{Zn}_5\text{L}_4^{2+}$ with a Ln(III) ion to form the $\text{LnZn}_4\text{L}_4^{3+}$. The $\text{LnZn}_4\text{L}_4^{3+}$ could then react with a $\text{Zn}_5\text{L}_4^{2+}$, displacing the central Zn(II) ion to form the $\text{LnZn}_8\text{L}_8^{3+}$ sandwich complex. This $\text{LnZn}_8\text{L}_8^{3+}$ sandwich complex could serve as a template for the $\text{LnZn}_{16}\text{L}_{16}^{3+}$, which would invoke the $\text{Zn}_5\text{L}_4^{2+}$ cannibalization reaction to obtain the eight ligands and eight Zn(II) needed to generate the $[24\text{-MC}_{\text{Zn(II),L-8}]$ motif. Additionally, the $\text{LnZn}_4\text{L}_4^{3+}$ could serve as a template for forming the $\text{LnZn}_{12}\text{L}_{12}^{3+}$ through a similar cannibalization reaction. The $\text{LnZn}_{12}\text{L}_{12}^{3+}$ could react with a

$\text{Zn}_5\text{L}_4^{2+}$ through a central metal substitution reaction to generate the $\text{LnZn}_{16}\text{L}_{16}^{3+}$.

The reactivity of the $\text{Zn}_5\text{L}_4^{2+}$ with Ln(III) ions in different solvents supports this mechanism. ^1H NMR and ESI-MS data show that $\text{Zn}_5\text{L}_4^{2+}$ conversion to the $\text{LnZn}_4(\text{picHA})_4^{3+}$, $\text{LnZn}_5(\text{picHA})_5^{3+}$,⁵⁶ and $\text{LnZn}_8(\text{picHA})_8^{3+}$ proceeds readily at room temperature, effectively reaching equilibrium after 24 h based on the minimal changes in the spectra after heating at 65 °C. (Figure 7 and Supporting Information Figures S5–S11). Likewise the $\text{LnZn}_5(\text{picHA})_5^{3+}$ appears in DMF, methanol, and DMF/pyridine upon reacting at room temperature. This facile assembly at room temperature is consistent with the $\text{LnZn}_4\text{L}_4^{3+}$, $\text{LnZn}_5\text{L}_5^{3+}$, and $\text{LnZn}_8\text{L}_8^{3+}$ being formed through a reaction with a low activation energy. It seems reasonable that central metal substitution or the central metal displacement reactions would have such low activation energies as they would involve the disruption of only four labile dative bonds. In contrast, the assembly of the $\text{LnZn}_{12}(\text{picHA})_{12}^{3+}$ and $\text{LnZn}_{16}(\text{picHA})_{16}^{3+}$ requires heating to reach equilibrium within 24 h (Figure 7 and Supporting Information Figures S7, S8, and S11). These differences suggest that there is a reasonably large activation energy for forming the $\text{LnZn}_{12}(\text{picHA})_{12}^{3+}$ and $\text{LnZn}_{16}(\text{picHA})_{16}^{3+}$ that is not present for the $\text{LnZn}_4(\text{picHA})_4^{3+}$, $\text{LnZn}_5(\text{picHA})_5^{3+}$, or $\text{LnZn}_8(\text{picHA})_8^{3+}$. The cannibalization reaction of the $\text{Zn}_5\text{L}_4^{2+}$ invoked to generate the eight Zn(II) and picHA ligands for the $[24\text{-MC}_{\text{Zn(II),picHA-8}]$ should possess a greater activation energy than central metal substitution or displacement. Therefore, the different temperatures required for assembling the $\text{LnZn}_{12}\text{L}_{12}^{3+}$ and $\text{LnZn}_{16}\text{L}_{16}^{3+}$ is consistent with the proposed assembly pathway. It should be noted that no evidence has been obtained to support that the $[24\text{-MC}_{\text{Zn(II),L-8}]$ species persists in the absence of the templating $\text{M}(\text{N})[12\text{-MC}_{\text{Zn(II),L-4}]^{\text{N}+}$.

Solution Stability. The stability of the LnMCs relative to the $\text{Zn}_5\text{L}_4^{2+}$ was assessed to gain insight into the utilization of the complexes in solution applications. The titrations of $\text{Ln}(\text{NO}_3)_3$ to $\text{Zn}_5(\text{picHA})_4(\text{OTf})_2$ show that the $\text{Zn}_5(\text{picHA})_4^{2+}$ has a similar thermodynamic stability as the LnMCs because residual $\text{Zn}_5(\text{picHA})_4^{2+}$ remains once the $\text{Ln}(\text{NO}_3)_3$ is added, even with an excess of $\text{Ln}(\text{NO}_3)_3$ for most of these titrations.⁵⁶ This greater thermodynamic stability with larger lanthanides is consistent with the trends in Ln(III) $[15\text{-MC}_{\text{Cu(II),pheHA-5}]^{3+}$ complexes in aqueous conditions.⁵⁹ The conversion to the $\text{YZn}_4(\text{picHA})_4^{3+}$ in 9:1 DMF/pyridine nearly proceeds to completion, though the $\text{YZn}_4(\text{quinHA})_4(\text{NO}_3)_3$ generates about 20% $\text{Zn}_5(\text{picHA})_4^{3+}$ upon dissolution after 26 h. In addition, the $\text{LnZn}_5(\text{picHA})_5^{3+}$, $\text{LnZn}_8(\text{picHA})_8^{3+}$, and $\text{Ln}_2\text{Zn}_9(\text{quinHA})_{10}(\text{OH})^{3+}$ undergo rearrangements to the $\text{Zn}_5(\text{picHA})_4^{2+}$ at room temperature over the period of hours to days. Interestingly, similar time scales are necessary to replace the central ion in $\text{Ca}(\text{II})[15\text{-MC}_{\text{Cu(II),pheHA-5}]^{3+}$ complexes with the thermodynamically preferred Ln(III) ions.⁶¹ Importantly, the rearrangement of the LnMCs to the $\text{Zn}_5(\text{picHA})_4^{2+}$ demonstrates that coordination of the central Ln(III) ion is kinetically unstable in these LnMCs at room temperature. Promisingly, as the rearrangement to the $\text{Zn}_5(\text{picHA})_4^{2+}$ is relatively slow, solution processing of the complexes and incorporation into ordered assemblies and networks may still be feasible.

Unlike the other LnMCs, the $\text{LnZn}_{16}(\text{picHA})_{16}^{3+}$ complexes with middle Ln(III) ions, such as Y(III), are stable kinetically in a variety of organic solvents at room temperature.²⁹ No $\text{Zn}_5(\text{picHA})_4^{2+}$ is observed by ESI-MS in methanol or pyridine

over many days. With the very large or very small Ln(III) ions such as La(III) and Yb(III), partial decomposition is evident in the trace $\text{Zn}_5(\text{picHA})_4^{2+}$ that grows in over the time period of hours to days in pyridine. The kinetic stability of the $\text{LnZn}_{16}(\text{picHA})_{16}^{3+}$ relative to the other LnMCs is likely a result of the decomposition mechanism. $\text{LnZn}_4\text{L}_4^{3+}$, $\text{LnZn}_5\text{L}_5^{3+}$, and $\text{LnZn}_8\text{L}_8^{3+}$ conversion to the $\text{Zn}_5\text{L}_4^{2+}$ involves central metal substitution, a kinetically facile reaction. In contrast, $\text{LnZn}_{16}\text{L}_{16}^{3+}$ conversion to the $\text{Zn}_5\text{L}_4^{2+}$ involves removal of Zn(II) and picHA ligands from the $[\text{24-MC}_{\text{Zn(II),L}}\text{-8}]$, which is presumably has a higher activation energy.

CONCLUSION

The field of coordination driven assembly has established that high symmetry macrocycles and polyhedra can be prepared by design when the building block geometries are compatible with the polynuclear supramolecular complex. Building blocks that deviate from these design principles can introduce complexity, as multiple assemblies can result from identical building blocks through equilibria that are difficult to understand or control because each construct possesses geometric strain. This work has helped to identify the role of symmetry incompatible building blocks in generating these promiscuous assembly equilibria. Moreover, it was recognized that open metal sites on these symmetry-incompatible building blocks serve a crucial role in obtaining and controlling solvent dependent assembly equilibria. More than eight LnMCs were shown to assemble in five different solutions using picHA, Zn(II), and Ln(III). Selectivity in their assembly is imposed by the preferential interaction of the solvent with the metal ions through hard-soft interactions and by the proclivity of water to form bridging hydroxide moieties.

Understanding these complex assembly equilibria using symmetry incompatible building blocks is beneficial for the design of functional multiple-component complexes and systems. The requirements of symmetry compatible building blocks can rigidly require certain metal ions to provide the appropriate coordination geometry, such as square-planar Pd(II) or Pt(II) ions to provide a 90° vertex. However, the inclusion of other metal ions may be necessary to provide the appropriate magnetic, spectroscopic, catalytic, or electrochemical properties for a particular application. For example, our interest in Ln(III) luminescence using LnMCs prompted the utilization of Zn(II) ring ions to avoid quenching through the *d-d* transitions of Cu(II) or Ni(II). In addition, responsive assemblies transition from one polynuclear complex to another triggered by molecular recognition hold promise in sensing or other systems chemistry applications. We expect that symmetry incompatible building blocks will be a reliable approach for generating responsive systems.

ASSOCIATED CONTENT

Supporting Information

Crystallographic CIF files, $\text{Dy(III)(NO}_3)_2[\text{15-MC}_{\text{Zn(II), quinHA}^-}\text{S}](\text{NO}_3)_3$ synthesis and crystal structure data, additional mass spectra and NMR on metallacrown assembly and stability, and proposed structure of the $\text{LnZn}_{12}(\text{picHA})_{12}(\text{DMF})_4^{3+}$. This material is available free of charge via the Internet at <http://pubs.acs.org>. Crystallographic data is available from the Cambridge Crystallographic Data Center using requisition numbers 878969 and 981753–981755.

AUTHOR INFORMATION

Corresponding Author

*E-mail: vlpec@umich.edu.

Notes

The authors declare no competing financial interest.

ACKNOWLEDGMENTS

We thank the National Science Foundation (CHE-0717098 and CHE-1057331) for funding. X-ray instrumentation was funded by the National Science Foundation (CHE-0840456).

REFERENCES

- (1) Chakrabarty, R.; Mukherjee, P. S.; Stang, P. J. *Chem. Rev.* **2011**, *111*, 6810–918.
- (2) Holliday, B. J.; Mirkin, C. A. *Angew. Chem., Int. Ed.* **2001**, *40*, 2022–2043.
- (3) Albrecht, M. *Chem. Rev.* **2001**, *101*, 3457–3497.
- (4) Yoshizawa, M.; Klosterman, J. K.; Fujita, M. *Angew. Chem., Int. Ed.* **2009**, *48*, 3418–38.
- (5) Pluth, M. D.; Bergman, R. G.; Raymond, K. N. *Acc. Chem. Res.* **2009**, *41*, 1650–1659.
- (6) Ono, K.; Yoshizawa, M.; Akita, M.; Kato, T.; Tsunobuchi, Y.; Ohkoshi, S.-i.; Fujita, M. *J. Am. Chem. Soc.* **2009**, *131*, 2782–2783.
- (7) Sun, W.-Y.; Kusakawa, T.; Fujita, M. *J. Am. Chem. Soc.* **2002**, *124*, 11571–11572.
- (8) Gianneschi, N. C.; M, M. S., III; Mirkin, C. A. *Acc. Chem. Res.* **2005**, *38*, 825–837.
- (9) Frischmann, P. D.; Guieu, S.; Tabeshi, R.; MacLachlan, M. J. *J. Am. Chem. Soc.* **2010**, *132*, 7688–7675.
- (10) Hui, J. K. H.; MacLachlan, M. J. *Coord. Chem. Rev.* **2010**, *254*, 2363–2390.
- (11) Li, D.; Zhou, W.; Landskron, K.; Sato, S.; Kiely, C. J.; Fujita, M.; Liu, T. *Angew. Chem., Int. Ed.* **2011**, *50*, 5182–7.
- (12) Inokuma, Y.; Arai, T.; Fujita, M. *Nat. Chem.* **2010**, *2*, 780–783.
- (13) Dinolfo, P. H.; Hupp, J. T. *Chem. Mater.* **2001**, *13*, 3113–3125.
- (14) Slone, R. V.; Benkstein, K. D.; Belanger, S.; Hupp, J. T.; Guzei, I. A.; Rheingold, A. L. *Coord. Chem. Rev.* **1998**, *171*, 221–243.
- (15) Imbert, D.; Cantuel, M.; Bunzli, J.-C. G.; Bernardinelli, G.; Piguet, C. *J. Am. Chem. Soc.* **2003**, *125*, 15698–15699.
- (16) Zaleski, C. M.; Depperman, E. C.; Kampf, J. W.; Kirk, M. L.; Pecoraro, V. L. *Inorg. Chem.* **2006**, *45*, 10022–10024.
- (17) Affronte, M.; Carretta, S.; Timco, G. A.; Winpenny, R. E. *Chem. Commun.* **2007**, 1789–97.
- (18) Piotrowski, H.; Severin, K. *Proc. Natl. Acad. Sci. U. S. A.* **2002**, *99*, 4997–5000.
- (19) Fujita, M. *Chem. Soc. Rev.* **1998**, *27*, 417.
- (20) Caulder, D. L.; Raymond, K. N. *Acc. Chem. Res.* **1999**, *32*, 975–982.
- (21) Pecoraro, V. L. *Inorg. Chim. Acta* **1989**, *155*, 171–173.
- (22) Lah, M. S.; Kirk, M. L.; Hatfield, W.; Pecoraro, V. L. *J. Chem. Soc., Chem. Commun.* **1989**, 1606–1608.
- (23) Lah, M. S.; Pecoraro, V. L. *J. Am. Chem. Soc.* **1989**, *111*, 7258–7259.
- (24) Stemmler, A. J.; Kampf, J. W.; Pecoraro, V. L. *Inorg. Chem.* **1995**, *34*, 2271–2272.
- (25) Pecoraro, V. L.; Stemmler, A. J.; Gibney, B. R.; Bodwin, J. J.; Wang, H.; Kampf, J. W.; Barwinski, A. *Prog. Inorg. Chem.* **1997**, *45*, 83–177.
- (26) Mezei, G.; Zaleski, C. M.; Pecoraro, V. L. *Chem. Rev.* **2007**, *107*, 4933–5003.
- (27) Zaleski, C. M.; Depperman, E. C.; Dendrinou-Samara, C.; Alexiou, M.; Kampf, J. W.; Kessissoglou, D. P.; Kirk, M. L.; Pecoraro, V. L. *J. Am. Chem. Soc.* **2005**, *127*, 12862–12872.
- (28) Boron, T. T., 3rd; Kampf, J. W.; Pecoraro, V. L. *Inorg. Chem.* **2010**, *49*, 9104–9106.
- (29) Jankolovits, J.; Andolina, C. M.; Kampf, J. W.; Raymond, K. N.; Pecoraro, V. L. *Angew. Chem., Int. Ed.* **2011**, *50*, 9660–4.

- (30) Trivedi, E. R.; Eliseeva, S. V.; Jankolovits, J.; Olmstead, M. M.; Petoud, S.; Pecoraro, V. L. *J. Am. Chem. Soc.* **2014**, *136*, 1526–1534.
- (31) Tegoni, M.; Tropiano, M.; Marchio, L. *Dalton Trans.* **2009**, 6705–6708.
- (32) Jankolovits, J.; Lim, C.-S.; Mezei, G.; Kampf, J. W.; Pecoraro, V. L. *Inorg. Chem.* **2012**, *51*, 4527–4538.
- (33) Grant, J. T.; Jankolovits, J.; Pecoraro, V. L. *Inorg. Chem.* **2012**, *51*, 8034–8041.
- (34) Severin, K. *Coord. Chem. Rev.* **2003**, *245*, 3–10.
- (35) Bodwin, J. J.; Pecoraro, V. L. *Inorg. Chem.* **2000**, *39*, 3434–3435.
- (36) Pavlishchuk, A. V.; Kolotilov, S. V.; Zeller, M.; Shvets, O. V.; Fritsky, I. O.; Lofland, S. E.; Addison, A. W.; Hunter, A. D. *Eur. J. Inorg. Chem.* **2011**, *2011*, 4826–4836.
- (37) Lim, C. S.; Jankolovits, J.; Kampf, J. W.; Pecoraro, V. L. *Chem. Asian. J.* **2010**, *5*, 46–49.
- (38) Moon, M.; Kim, I.; Lah, M. S. *Inorg. Chem.* **2000**, *39*, 2710–2711.
- (39) Stemmler, A. J.; Kampf, J. W.; Pecoraro, V. L. *Angew. Chem., Int. Ed. Engl.* **1996**, *35*, 2841–2843.
- (40) Traditional metallacrown nomenclature is used in this work when necessary to convey structural meaning, following the formula $M(N)[\# \text{ ring atoms-MC}_{M'(N')L} \# \text{ ring oxygens}](\text{anions})(\text{coordinated ligands})$ where M is the central ion, N is the oxidation state of the central metal, MC is the abbreviation of metallacrown, M' is the ring ion, N' is the oxidation state of the ring ion, and L is the ligand. Thus, $Zn(II)[12-MC_{Zn(II),picHA-4}](OTf)_2$ is a metallacrown with a 12-membered ring containing four oxygen atoms, four Zn(II) ions in the ring, a Zn(II) central ion, and two triflate counteranions. In this work, abbreviated molecular formula are used to refer to specific complexes. When referring to a general complex where the anions or charge are unspecified, then the anions and/or charge are omitted and the charge is specified where appropriate. For example, $Zn_5(picHA)_4(OTf)_2$ refers to a $Zn(II)[12-MC_{Zn(II),picHA-4}](OTf)_2$ complex, whereas $Zn_5L_4^{2+}$ refers to the general +2 charged cation with any picHA ligand derivative, regardless of the associated anion.
- (41) Gibney, B. R.; Kessissoglou, D. P.; Kampf, J. W.; Pecoraro, V. L. *Inorg. Chem.* **1994**, *33*, 4840–4849.
- (42) Dallavalle, F.; Tegoni, M. *Polyhedron* **2001**, *20*, 2697–2704.
- (43) Stemmler, A. J.; Kampf, J. W.; Kirk, M. L.; Atasi, B. H.; Pecoraro, V. L. *Inorg. Chem.* **1999**, *38*, 2807–2817.
- (44) Seda, S. H.; Janczak, J.; Lisowski, J. *Inorg. Chem. Commun.* **2006**, *9*, 792–796.
- (45) Dallavalle, F.; Remelli, M.; Sansone, F.; Bacco, D.; Tegoni, M. *Inorg. Chem.* **2010**, *49*, 1761–72.
- (46) Tegoni, M.; Remelli, M. *Coord. Chem. Rev.* **2012**, *256*, 289–315.
- (47) Mugridge, J. S.; Fiedler, D.; Raymond, K. N. *J. Coord. Chem.* **2010**, *63*, 2779–2789.
- (48) Caulder, D. L.; Raymond, K. N. *J. Chem. Soc., Dalton Trans.* **1999**, 1185–1200.
- (49) Fujita, M.; Sasaki, O.; Mitsuhashi, T.; Fujita, T.; Yazaki, J.; Yamaguchi, K.; Ogura, K. *Chem. Commun.* **1996**, 1535.
- (50) Kilbas, B.; Mirtschin, S.; Scopelliti, R.; Severin, K. *Chem. Sci.* **2012**, *3*, 701.
- (51) Suzuki, K.; Kawano, M.; Fujita, M. *Angew. Chem., Int. Ed.* **2007**, *46*, 2819–2822.
- (52) Mamula, O.; Lama, M.; Stoeckli-Evans, H.; Shova, S. *Angew. Chem., Int. Ed.* **2006**, *45*, 4940–4944.
- (53) Baxter, P. N. W.; Khoury, R. G.; Lehn, J.-M.; Baum, G.; Fenske, D. *Chem.—Eur. J.* **2000**, *6*, 4140–4148.
- (54) Zarra, S.; Clegg, J. K.; Nitschke, J. R. *Angew. Chem., Int. Ed.* **2013**, *52*, 4837–4840.
- (55) Jankolovits, J.; Kampf, J. W.; Pecoraro, V. L. *Polyhedron* **2013**, *52*, 491–499.
- (56) Jankolovits, J.; Kampf, J. W.; Pecoraro, V. L. *Inorg. Chem.* **2013**, *52*, 5063–76.
- (57) *Crystalclear 2.0*; Rigako Corporation: Tokyo, Japan.
- (58) Sheldrick, G. M. *Acta Crystallogr.* **2008**, *A64*, 112–122.
- (59) Tegoni, M.; Furlotti, M.; Tropiano, M.; Lim, C.-S.; Pecoraro, V. L. *Inorg. Chem.* **2010**, *49*, 5190–5201.
- (60) *Discovery Studio Modeling Environment*, release 2.5; Accelrys Software Inc.: San Diego, CA, 2009.
- (61) Lim, C.-S.; Tegoni, M.; Jakusch, T.; Kampf, J. W.; Pecoraro, V. L. *Inorg. Chem.* **2012**, *51*, 11533–40.